



Philipp Hackl BSc

Analysis of Switching Overvoltages of a 110 kV Circuit Breaker with EMTP

MASTER'S THESIS

to achieve the university degree of

Diplom-Ingenieur

Master's degree programme: Electrical Engineering

submitted to

Graz University of Technology

Supervisor

Ass.Prof. Dipl.-Ing. Dr.techn. Katrin Friedl

Institute of Electrical Power Systems

Univ.-Prof. DDipl.-Ing. Dr.techn. Robert Schürhuber

Graz, July 2020

AFFIDAVIT

I declare that I have authored this thesis independently, that I have not used other than the declared sources/resources, and that I have explicitly indicated all material which has been quoted either literally or by content from the sources used. The text document uploaded to TUGRAZonline is identical to the present master's thesis.

Date

Signature

Contents

1. Abstract	3
2. Introduction	5
3. Theory	7
3.1. Classification of Voltage Stress	7
3.2. Circuit Breakers	7
3.2.1. Minimum Oil Circuit Breaker	8
3.2.2. SF6 Circuit Breaker	8
3.3. Switching in Power Systems	9
3.3.1. Total Clearing Time	9
3.3.2. Switching Arc	9
3.3.3. (Transient) Recovery Voltage	10
3.3.4. Pole-to-Clear Factor	10
3.3.5. Reignition	11
3.3.6. Current Copping	11
3.3.7. Controlled Switching	11
3.4. Voltage Measurement	13
3.4.1. Voltage Transformers	13
3.4.2. Voltage Dividers	13
3.5. Modelling for High Frequency	13
3.5.1. Transmission Line Model	13
3.5.2. Lossless Line Model	15
3.5.3. Inclusion of Losses	15
3.5.4. Travelling Waves	16
3.6. Frequency Dependence of Transmission Line Parameters	16
3.6.1. Skin-Effect	16
3.6.2. Proximity-Effect	17
3.6.3. Inductance	19
4. Measurement	21
4.1. Motivation	21
4.2. Measurement Setup	21
4.2.1. Entire Measurement Setup	21
4.2.2. Layout of the Measurement Area	21
4.2.3. Measurement Equipment and Short Circuit	24

4.3. Measurement Results	25
4.3.1. SF6 Circuit Breaker	25
4.3.2. Opening Process	25
4.3.3. Arc Voltage	26
4.3.4. Reignition	26
4.3.5. Fourier Transformation of Voltages	28
4.3.6. Minimum Oil Circuit Breaker	28
5. EMTP-Introduction	31
5.1. Simple Example	31
5.2. Cable Models	33
5.2.1. CP Model	33
5.2.2. FDQ Model	34
5.2.3. WB Model	34
5.2.4. Cable Data - Geometry Input	34
5.2.5. WB Fitter	36
5.2.6. Comparision of Cable Models	36
5.2.7. Influence of the Shield Earthing	40
5.3. Line Models	42
5.3.1. Line Rebuild	43
5.3.2. Geometry Input	43
5.3.3. Different Geometries	44
5.3.4. Comparison of Line Models	45
5.4. Busbar Model	47
5.5. Transformer Model	49
5.6. Peterson Coil	52
5.7. Voltage Divider	52
5.8. Switch Models	53
5.8.1. Ideal Breaker	53
5.8.2. Breaker for TRV	53
6. EMTP-Results	55
6.1. Simulation Model	55
6.2. Simulation Results	55
6.2.1. Switching Voltages	55
6.2.2. Fourier Transformation of Switching Voltages	56
6.3. Sensitivity Analysis	58
6.3.1. Bus Bar Model	58
6.3.2. Transformer Model	58
6.3.3. Cable Model	59
6.3.4. Line Model	60
6.3.5. Grid Impedance	60
6.3.6. Voltage Dividers	61

6.4. Comparison of Measurement with Simulation	62
6.4.1. Influence Grid Impedance	62
6.4.2. Neglection of Components in Substation	62
6.4.3. Influence Circuit Breaker for TRV	63
7. Conclusion	65
Appendices	I
A. Appendix	I

Abbreviations

AC	alternating current
APL	aluminium-polyethylene-laminated
CP	constant parameters
DC	direct current
EMTP	electromagnetic transient program
FD	frequency depending
FDQ	frequency depending Q matrix
FFT	Fast Fourier Transformation
GIL	gas insulated lines
GIS	gas insulated substation
HDPE	high-density polyethylene
Hz	Hertz
p.u.	per unit
RV	recovery voltage
SF6	sulphur hexafluoride
TRV	transient recovery voltage
WB	wideband
XPE	cross-linked polyethylene

Nomenclature

C'	capacitance per unit length
δ	skin depth
f_g	resonance frequency
G'	conductance per unit length
$\underline{\gamma}$	complex propagation constant
k_{pp}	pole-to-clear factor
L'	inductance per unit length
λ	wavelength
μ_0	permeability constant
μ_r	relative permeability
R'	resistance per unit length
ρ	material resistivity
τ	propagation delay
v_p	propagation speed
v_{wave}	wave propagation velocity
\underline{Z}_c	characteristic impedance
Z_s	surge impedance

1. Abstract

Overvoltages often occur in high voltage systems due to switching operations. Usually these are superimpositions of high frequency transient voltages and the operating frequency voltages. These voltages have to stay within the limits defined by insulation coordination standards and equipment ratings. So they have been investigated to ensure these properties. In the course of a renewal of a substation, short circuit tests of 110 kV circuit breakers were found. The switching overvoltages occurring during fault clearing were measured. The aim of this thesis is to simulate the network structure in the simulation program EMTP (Electromagnetic Transient Program) and to verify the results of the measurements. Afterwards the influence of the different components should be investigated and the main parameters for the occurring voltages should be found.

For this purpose, the occurring effects are discussed at the beginning of the thesis and the performed measurement are described in detail. Then the different line and cable models of EMTP are analysed in detail. Finally the simulation is explained and the results are compared with the measurement.

The results show that the transient recovery voltage at the circuit breaker are reproduced well and that the two different transient voltages are clearly visible. It turns out that one transient voltage can be traced back to the grid impedance and the overhead line connecting the substation. The other transient is a result of the interaction of the transformer and the components installed at its secondary side. Based on this work, the parameter study can be done in more detail.

2. Introduction

In power engineering, substations are used to adjust the voltage levels, but also as distribution points for electrical energy. One of the most important components here is the circuit breaker. It is the only component which can safely switch off a short circuit, whereby it is able to extinguish the arc and stop the current flow. However, by interrupting the current flow, the stored magnetic energy must be converted. This leads to switching overvoltages with transient voltages which have higher amplitudes and frequencies than the operating voltage.

In order to investigate this process, short circuit measurements in a substation were made. Therefore a measurement setup was installed where the occurring switching overvoltages after clearing a short circuit were measured. Two distinct transient voltages and other effects were identified from the measurement results. In order to find out which components were mainly responsible for this result, this experiment shall be simulated with the simulation program EMTP from powersys.

As there are several possibilities for modelling overhead lines and cables in the simulation program, these are explained in more detail and compared with each other. Furthermore, a sensitivity analysis is carried out to find the parameters that affect the result the most. The simulation result should then be compared with the measurement result and the possible reasons for the deviation explained.

In the beginning of the thesis the theory for switching in power systems and the transmission line model are discussed. Then the measurement is explained and the results are shown. Subsequently, the possible models for each component were introduced. Finally, the simulation model with the simulation results compared with the measurement are discussed.

3. Theory

3.1. Classification of Voltage Stress

Voltage stresses can be first classified roughly into steady state and transient events. A further distinction can be made between the time and the frequency range. This leads to a division of the transient stresses into slow, fast and very fast processes. The fast and very fast processes occur mainly in GIS (gas insulated substation) and in the case of lightning strikes. The steady state voltages are mostly caused by temporary effects of the grid. In this thesis, switching voltages of an outdoor installation are investigated, which are in the slow transient range. Frequencies of several Hz (Hertz) up to a few kHz are expected. The figure 3.1 shows an overview of this voltage classification. [1]

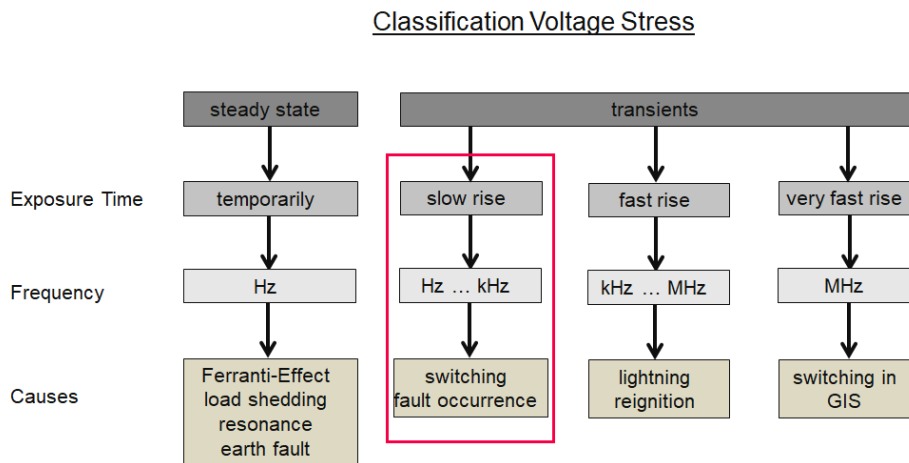


Figure 3.1.: Classification of Voltage Stress

3.2. Circuit Breakers

A circuit breaker is a switch that ensures the reliable interruption of operating and short circuit currents in electrical power transmission. It must also ensure the safe insulation of the recovery voltage. When operating AC (alternating current), the arcing is extinguished at zero current crossing to achieve the insulating distance between the contacts for the necessary dielectric strength. This can be achieved by cooling or by increasing the arc voltage.

Due to the different voltage levels and applications, the following different technologies have developed historically:

- Air Circuit Breaker
- Vacuum Circuit Breaker
- Bulk Oil Circuit Breaker
- Minimum Oil Circuit Breaker
- SF6 (sulphur hexafluoride) Circuit Breaker

In the high voltage technology for networks over 100 kV, the minimum oil circuit breaker and the SF6 circuit breaker have been established. Since these were used for the measurements of this thesis, they will be described briefly below. [2]

3.2.1. Minimum Oil Circuit Breaker

The first efficient circuit breakers were bulk oil breakers, where the produced arc burns in the oil when the contacts are opened. The oil withdraw the energy from the arc by vaporizing, decomposing and heat transfer until the arc is extinguished. Because of the limited performance and the high risk of explosion, the minimum oil circuit breaker was developed.

Here, the arc burns in a tight arc extinguishing chamber and the passing oil can be used more effective for extinguishing. With the upcoming SF6 circuit breakers, the minimum oil circuit breakers lost their importance. However, due to their long lifetime, they are still partially installed.

3.2.2. SF6 Circuit Breaker

This circuit breaker uses SF6 as insulation instead of air, oil or vacuum. SF6 is an artificial gas which is colourless, odourless and tasteless, non-toxic, non-explosive and non-flammable. It is relatively easy to manufacture with a moderate price and the main advantages are the high thermal conductivity and the high dielectric strength. Therefore it is used in gas insulated switchgear (GIS), circuit breakers and GIL (gas insulated lines). The main disadvantage is that SF6 is a strong greenhouse gas and therefore the usage has to be strictly controlled.

The operation of the SF6 circuit breaker is similar to that of the minimum oil circuit breaker, whereby the occurring arc at the opening must be extinguished. The gas is blown under pressure into the arc extinguishing chamber. As it flows past, it extracts heat from the arc and cools it in this way. After the arc has extinguished at the current zero crossing, the insulation distance is dielectrically solidified by the SF6.

3.3. Switching in Power Systems

3.3.1. Total Clearing Time

If a fault occurs in the power system, the current has to be interrupted by using a circuit breaker. However, this does not happen infinitely fast. The fault must first be detected, the release mechanism be tripped, the circuit breaker be opened and then the resulting arc be extinguished. The fault is only eliminated after the arc has been extinguished. Each of these operations takes a certain amount of time, where the sum of these is known as the total clearing time. Figure 3.2 summarizes all times and actions.

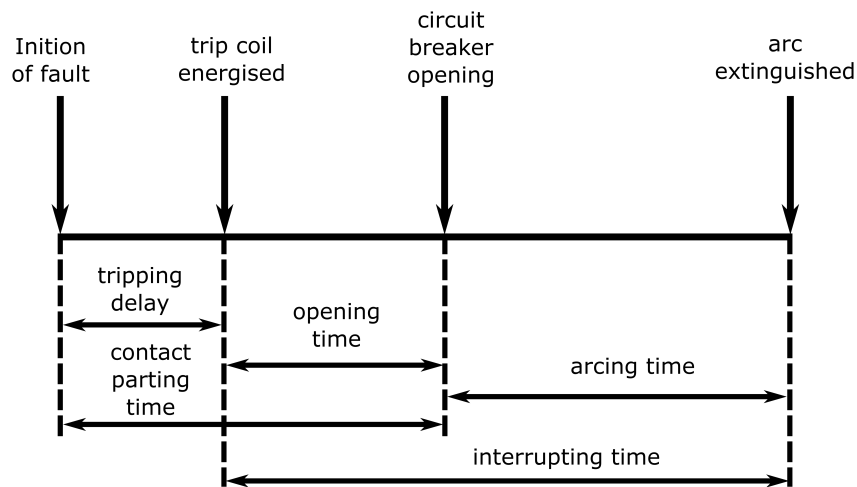


Figure 3.2.: Total Clearing Time [3]

3.3.2. Switching Arc

If a current flows through a circuit breaker and will be opened, it continues to flow via an arc. This is the case because the magnetic energy, stored in the power system, continues to drive a current to be dissipated. Due to the enormous energy, the contacts heat up as much that they begin to evaporate. This matter is under enormous heat, causing molecules to separate into atoms and then even positive ions and electrons. The mixture of these free electrons and ions is called the plasma state and is highly conductive. The current flows through this arc plasma after the contact separation.

To interrupt this current channel, it must be cooled or the arc field strength must be increased. An arc voltage increase can be achieved by separation into partial arcs. In this case the cathode and anode drop is used for each one. Another possibility is the so called arcing quenching. In this case, the plasma is cooled down at zero current crossing in AC to such an extent that no more ignition occurs afterwards.

3.3.3. (Transient) Recovery Voltage

If a fault is cleared with a circuit breaker, a voltage is formed across the two poles, which is called RV (recovery voltage). This voltage has typically a power frequency component and one with a higher frequency, the so called TRV (transient recovery voltage). It can occur in various forms and in practice the frequency is in the range of a few kHz. If there are still enough ionized charge carriers in the gap between the contacts, the arc will reignite due to the TRV. The switching process is only successful if the recovery voltage does not lead to new ignitions. The figure 3.3 shows a switching operation of a purely inductive circuit. The time in which the arc burns and the transient recovery voltage can be seen clearly. [4]

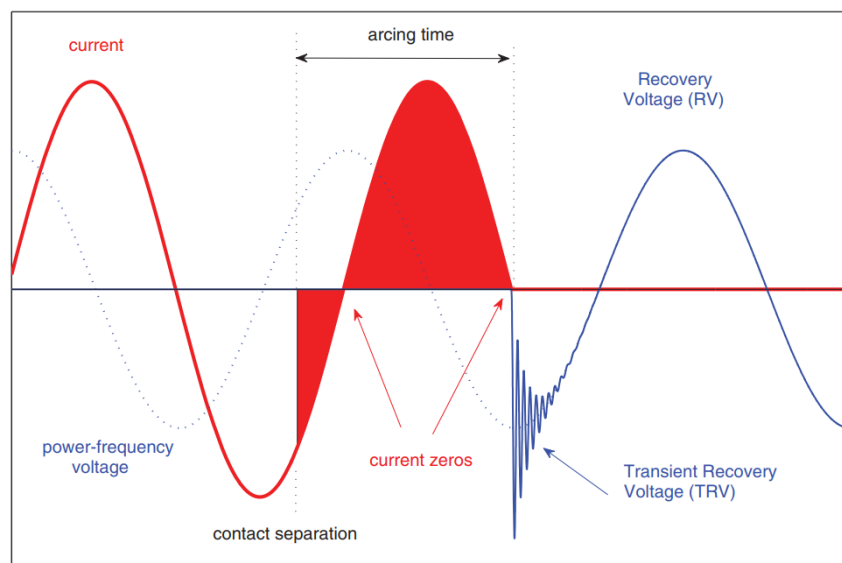


Figure 3.3.: Current Interruption in a Purely Inductive AC Circuit [5]

3.3.4. Pole-to-Clear Factor

In a multi-phase system, the zero crossings at which the arcs are extinguished do not occur simultaneously. This leads to different interruption times of each phase which results in a temporarily asymmetrical fault. As a result, the recovery voltage will have overvoltages that exceed the operating voltage. The ratio between the recovery voltage and the pre-fault power frequency voltage is given by the dimensionless k_{pp} (pole-to-clear factor). This factor strongly depends on the neutral point treatment, whereby the first-pole-to-clear factor is commonly used to describe the influence. The second- and third-pole-to-clear factor indicates the momentary recovery voltage of the other phases. After interruption of the last two poles, the RV across all poles are restored to 1 p.u.

Table 3.1.: Pole Factors of Different Neutral Point Treatment[6]

neutral point treatment	k_{pp1}	k_{pp2}	k_{pp3}
solidly grounded	1	1	1
effectively grounded	1.3	1.27	1
isolated/resonantly grounded	1.5	0.86	0.86

3.3.5. Reignition

There are two possible reasons for the occurrence of reignitions, which will be discussed in the following. These are thermal reignitions and the dielectric reignitions.

Thermal Reignition

In the case of thermal reignition, the arc channels are still conductive after the current interruption at current zero crossing. This is the case because the previously generated arc plasma loses its conductivity very quickly, but too less that there is no current flow anymore. So energy will flow through this path, which again causes the channel to heat up. This will cause the channel to ignite again. As a remedy a good cooling after the current zero crossing is mandatory.

Dielectric Reignition

In the case of dielectric reignition the arc is already completely extinguished and the clearance path gains in dielectric strength. However, if the clearance solidification between the open contacts is lower than the transient recovery voltage, it may come to reignitions. This breakdown occurs later than the thermal reignition, but with a rapidly rising current.

3.3.6. Current Copping

Due to instabilities in the low-current arc the current can be forced to zero. This phenomenon is called chopping current, because typically the current is interrupted at a few amperes before zero crossing. As a result, the stored magnetic energy can lead to high overvoltages by charging the leakage capacitors. Figure 3.4 demonstrates the effects this chopping current can have on the TRV. As soon as the current is interrupted, the TRV starts to rise, but in this case with the same polarity as the arc voltage. The absolute maximum of the TRV without reignition is called recovery peak and it can be seen that it differs significantly.

3.3.7. Controlled Switching

Several approaches to prevent overvoltages during opening the contacts exist. One possibility is to use the control of the contact separating time. In this case the risk of

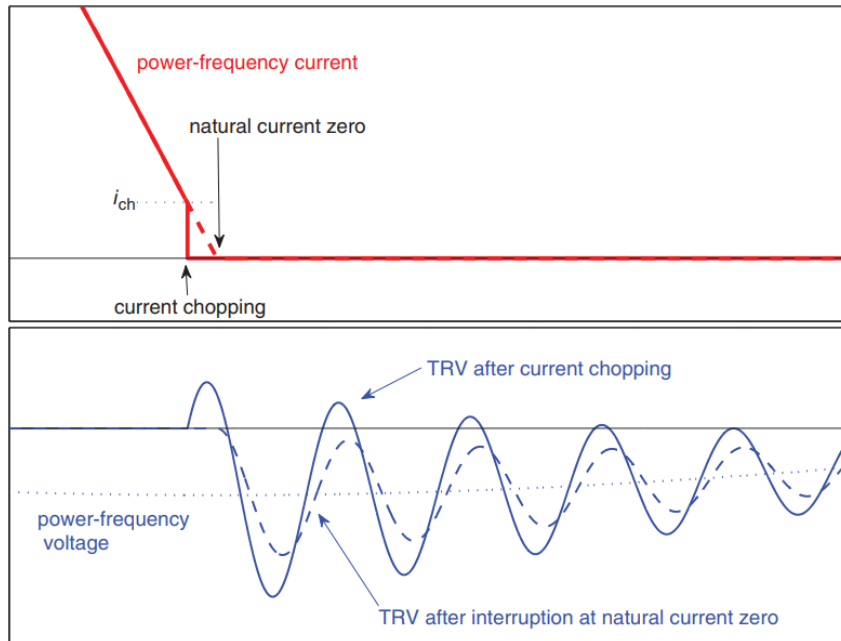


Figure 3.4.: Comparison of TRVs: with Current Chopping (drawn line) and without Current Chopping (dashed line) [5]

overvoltages due to reignition can occur if the contacts open too early. Since even surge arresters do not offer sufficient protection due to these steep voltage stresses, this time should be avoided. But by increasing the arcing time, overvoltages due to current chopping can occur. However, as these are usually not so critical, it is recommended to extend the arcing time by controlled opening. The perfect time window is located in the middle of these two areas, as shown in figure 3.5.

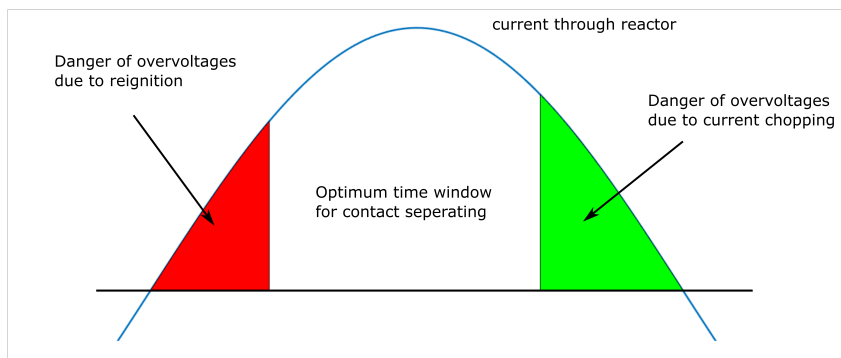


Figure 3.5.: Optimum Time Window for Contact Opening [3]

3.4. Voltage Measurement

3.4.1. Voltage Transformers

To measure high voltage, it must be transformed down to the measuring range of the available measuring instruments. This can be done with a so called voltage transformer. With an inductive voltage transformer the high voltage side feeds the primary winding and by adjusting the winding ratio the reduced voltage can be measured on the secondary side. For higher voltages, capacitive voltage transformers are used, whereby a capacitive voltage divider is connected in front of an inductive voltage transformer. There are also combined transformers, which can measure the voltage but also the current through the high voltage line.

The voltage transformers, as operating equipment of the electrical supply network, are primarily used to measure the operating frequency voltages. They must have a certain accuracy during normal operation and in the event of a fault they must be able to clearly identify it. This then leads to clarification of the fault.

3.4.2. Voltage Dividers

Another possibility to measure high voltage is to use voltage dividers. These are designed in such a way that the majority of the voltage drops at the high voltage component. Then a low voltage proportional to the high voltage can be measured. However, attention must be paid to the stray capacitances, whereby a resistive capacitive voltage divider can be used for alternating voltage. Furthermore, the correct terminating impedance must be ensured during the measurement to prevent reflections. With this technology it is also possible to measure non-operating frequency voltages.

3.5. Modelling for High Frequency

3.5.1. Transmission Line Model

If current carrying lines are in close distance and the conductor cross sections are not negligibly small, effects occur whose impacts are otherwise negligible. These effects can be found in overhead lines and high voltage cables, consequently joined together as transmission lines, and can be described by the following parameters.

- The R' (resistance per unit length) in Ω per unit length
- The L' (inductance per unit length) in Henry per unit length
- The C' (capacitance per unit length) in Farad per unit length
- The G' (conductance per unit length) of the dielectric material separating the two conductors in Siemens per unit length

The figure 3.6 shows the schematic of this transmission line for an infinitely small part. It can be seen that an inductance L' is formed by the conductor loop. Furthermore, the small distance between the conductors creates a capacitance C' to each other. If the insulating dielectric is not infinitely insulated, a leakage resistance G' has to be added. R' corresponds to the resistance of the conductor element and depends on the conductor material. [7]

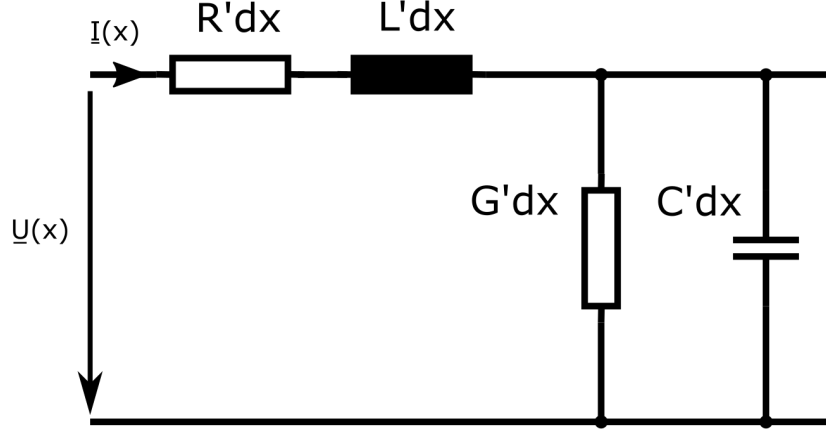


Figure 3.6.: Schematic Transmission Line

The behaviour can be described mathematically in the frequency domain with the Telegrapher's equations as follows. Here x is the distance in the direction of propagation of the transmission line and ω the angular frequency.

$$\frac{\partial V(x)}{\partial x} = -(R' + j\omega L') \underline{I}(x) \quad (3.1)$$

$$\frac{\partial I(x)}{\partial x} = -(G' + j\omega C') \underline{V}(x) \quad (3.2)$$

In the general case the loss terms, R' and G' , are both included. The full form of the Telegrapher's equations in second order where $\underline{\gamma}$ (complex propagation constant) is introduced become the following. Where s is the complex frequency parameter number.

$$\frac{\partial^2 V(x)}{\partial x^2} = \underline{\gamma}^2 \underline{V}(x) \quad (3.3)$$

$$\frac{\partial^2 I(x)}{\partial x^2} = \underline{\gamma}^2 \underline{I}(x) \quad (3.4)$$

$$\underline{\gamma} = \sqrt{(R' + sL')(G' + sC')} = \alpha + j\beta \quad (3.5)$$

To complete the most important equations of transmission line theory, the equations for the \underline{Z}_c (characteristic impedance) and the v_{wave} (wave propagation velocity) need to

be added.

$$\underline{Z}_c = \sqrt{\frac{R' + sL'}{G' + sC'}} \quad (3.6)$$

$$v_{\text{wave}} = \frac{\omega}{\beta} \quad (3.7)$$

3.5.2. Lossless Line Model

If the losses are neglected, the calculation of the characteristic impedance is reduced and is called Z_s (surge impedance). This becomes then a completely real value. Furthermore, the propagation constant is simplified and the v_p (propagation speed) is calculated as follows. The τ (propagation delay) can also be introduced.

$$Z_S = \sqrt{\frac{L'}{C'}} \quad (3.8)$$

$$v_p = \frac{1}{\sqrt{L'C'}} \quad (3.9)$$

$$\tau = l \cdot \sqrt{L'C'} \quad (3.10)$$

One way to model the transmission line model is to assume the parameters as constant. This leads to the prevention of convolution problems where losses are neglected in the beginning. The equivalent schematic results as shown in figure 3.7 where the values of the two current sources are given in the following equations. This model has a time domain decoupling effect on the interconnected networks. [8]

$$i_{1h} = \frac{v_2(t - \tau)}{Z_S} + i_2(t - \tau) \quad (3.11)$$

$$i_{2h} = \frac{v_1(t - \tau)}{Z_S} + i_1(t - \tau) \quad (3.12)$$

3.5.3. Inclusion of Losses

To take the losses into account, the transmission line is divided into two separate lossless lines with half of the propagation time. Between them a resistor with half the resistance value and at the ends with the quarter resistance value is added, as shown in figure 3.8. This approximation is acceptable if $Z_C \gg R$, which is sufficient for most of the cases. [8]

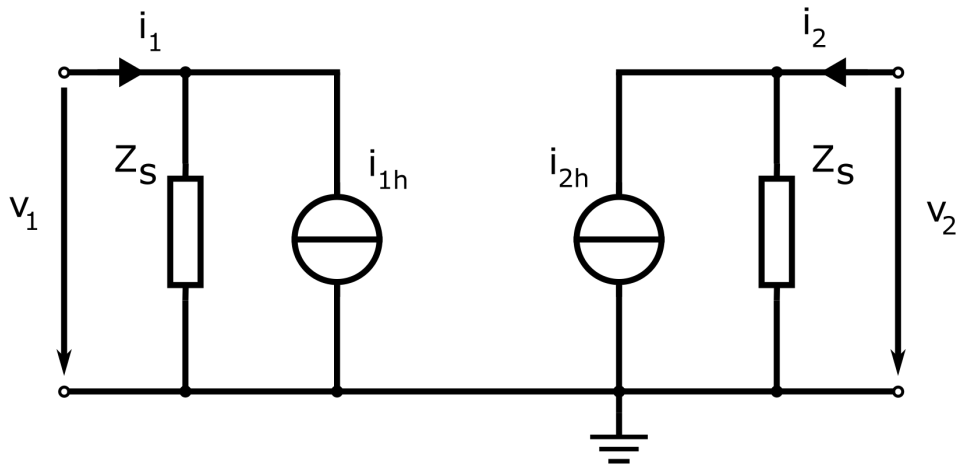


Figure 3.7.: Lossless Transmission Line Model for Time Domain

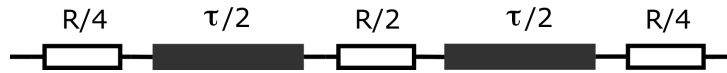


Figure 3.8.: Inclusion of Losses in Transmission Line Model

3.5.4. Travelling Waves

For fast transient stresses the propagation of travelling waves can no longer be neglected. This is the case because λ (wavelength) depends on the propagation speed v_p and frequency f . It is inversely proportional to the frequency and thus decreases as the frequency increases.

A travelling wave can be formed by switching operations or lightning strikes. It then propagates in both directions at the speed of propagation. It can be partially or completely reflected at the ends of the line or when it meets another characteristic impedance. These reflections subsequently superimpose the voltages and can lead to overvoltages.

$$\lambda = \frac{v_p}{f} \quad (3.13)$$

3.6. Frequency Dependence of Transmission Line Parameters

3.6.1. Skin-Effect

With DC (direct current) voltage, the current flow in a conductor is distributed uniformly over the cross-sectional area as shown in figure 3.9 on the left side. Thus, the entire cross-section can be used and the lowest possible resistance is obtained.

At AC voltage the current density across the conductor is no longer constant, but decreases towards the center of the conductor. The resistance of the conductor increases

because the current is displaced to the skin of the conductor and the effective cross section is less. In figure 3.9 this is well illustrated on the right side by the current density. Inside, marked in blue, the current density has decreased compared to DC and has increased strongly at the edge, recognizable by the red area. This happens because eddy currents are induced by the changing magnetic field. Thus the charge carriers are displaced into the skin of the conductor and at very high frequencies the electric field cannot penetrate the material at all to cause a current flow in the middle of the conductor.

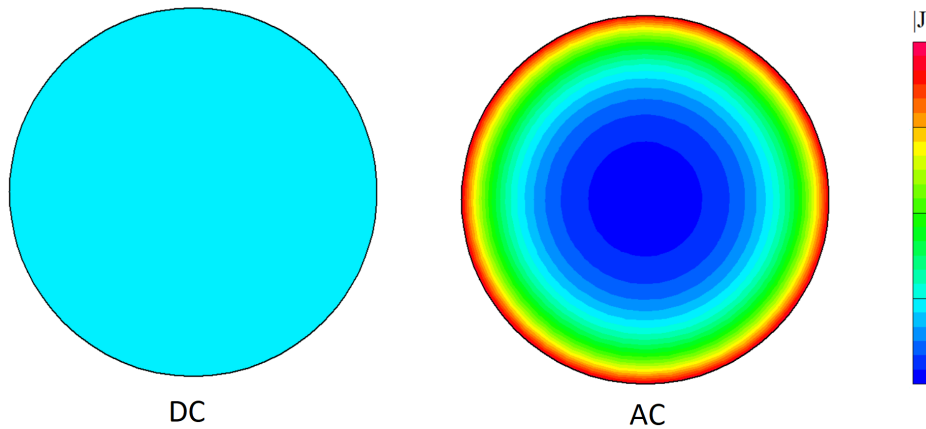


Figure 3.9.: Skin Effect - Current Density of DC (left) and AC (right)

An important measure of this is the so called δ (skin depth). It indicates how far the current flow can penetrate the material depending on the frequency. A conductor with a hollow core with the wall thickness δ has the same resistance as a solid conductor at alternating voltage. This occurs because the inner area of the conductor is current free. Figure 3.10 shows this skin depth at higher frequencies.

$$\delta = \sqrt{\frac{2\rho}{\omega\mu_0\mu_r}} \quad (3.14)$$

The skin depth δ can be calculated as a good approximation from the ρ (material resistivity), the frequency, the μ_0 (permeability constant) and the μ_r (relative permeability) as showed as equation. The table shows some calculated values for different frequencies of copper. It can be seen that the skin depth decreases with higher frequencies and as a consequence the effective resistance increases. [9]

3.6.2. Proximity-Effect

In comparison to the skin effect, which occurs with a single conductor, there is also an influence from other lines. This influence is called proximity effect and occurs especially

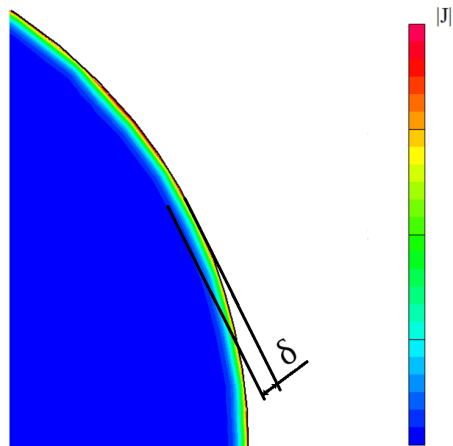


Figure 3.10.: Skin Effect - Skin Depth at Higher Frequencies

Table 3.2.: Skin Depth of Copper [9]

frequency	skin depth δ
50 Hz	9.38 mm
60 Hz	8.57 mm
500 Hz	2,97 mm
5 kHz	938 μm
10 kHz	660 μm
10 MHz	21 μm

with thick parallel running lines with low distance to each other and high frequencies. So this is interesting for inductors, transformers and also cables that are laid side by side. It leads to a dependency of the type of laying of cables based on the laying in a triangle or in a plane.

The alternating current creates an alternating magnetic field around a conductor and this induces eddy currents in the adjacent line. These dependent on the direction of the currents in the conductor and lead to a change in the current density distribution. As a result, as with the skin effect, the resistance and self inductance are influenced. [10]

3.6.3. Inductance

In electrical engineering, the inductance is often used as a central component and in the following the origin and dependencies will be discussed in more detail.

First of all, a distinction must be made between self inductance and mutual inductance. The mutual inductance M indicates the magnetic influence of electromagnetic induction on neighbouring electrical circuits. The self inductance L relates the rate of change of the electric current over time to the electric voltage. Without an addition, it is usually spoken about the self inductance.

The self inductance itself is further divided into an inner and an outer inductance. The outer inductance is dependent on the magnetic flux occurring outside the conductor. However, if the conductor has a not negligible cross-section, an inner inductance is also formed. This is dependent on the magnetic flux density and can be calculated in the simplest case with the following formula if the distribution is uniform. It is noticeable that with uniform current density distribution, this inductance does not depend on the diameter of the conductor.

$$L_{inner} = \frac{\mu_0 \mu_r l}{8\pi} \quad (3.15)$$

Due to the skin effect and the proximity effect, however, this current density distribution changes and the calculation of the internal inductance becomes more complex. This leads to a strong frequency dependence of the inner inductance, which is a not to be neglected factor especially for cables due to the large diameter of the cross section. The self inductance is then made up of the sum of the outer and inner inductance.

For a shielded single conductor cable, which is usually also called coaxial cable, the inductance is calculated from the sum of the two inner inductors and the outer inductance between the conductors. Whereby the outer inductance in the dielectric is frequency independent.

$$L_{outer} = \frac{\mu_0 \mu_r l}{2\pi} \cdot \ln \frac{D}{d} \quad (3.16)$$

It should also be mentioned that the inductance depends on the relative permeability number of the respective material. At high magnetic flux densities, saturation can occur, whereby this material constant can also decrease and lead to a non-linear behaviour.

4. Measurement

4.1. Motivation

Due to a renewal of a 110 kV switchgear, company representatives and scientific institutes decided to run tests directly on the old system before it will be dismantled. The new gas-insulated switchgear was already in operation and the whole old system served as a test field. For the measurements, a direct connection over about 100 km overhead line from another 220 kV substation was provided. Furthermore, a transformer was disconnected and used for this application.

One of these measurements was a test where a three-pole short circuit was switched to a circuit breaker and cleared by it. These measurements will be discussed in more detail in the following chapters.

4.2. Measurement Setup

4.2.1. Entire Measurement Setup

For the measurement, a short circuit is closed on a circuit breaker and then cleared by it. The occurring switching voltages are measured. For this purpose, a fast sampling must be carried out due to the transient processes.

A transformer with a specially for this purpose disconnected overhead line from a 220 kV transformer station to a second one was used. Subsequently, a construction cable was connected to supply the first feeder, which served as safety. A bus bar was then used to connect the investigated circuit breaker and the short-circuit. This test was executed with a minimum oil breaker and a SF6 breaker.

Figure 4.1 shows the entire measurement setup and in the following lines this measurement setup is described in more detail.

4.2.2. Layout of the Measurement Area

The following figure 4.2 shows the configuration of the measurement using the layout of the substation. It can be seen how the cable coming from the transformer supplies the two circuit breakers via the first feeder. The minimum oil circuit breaker and the SF6 breaker were connected separately. The necessary components for the voltage measurements were mounted accordingly.

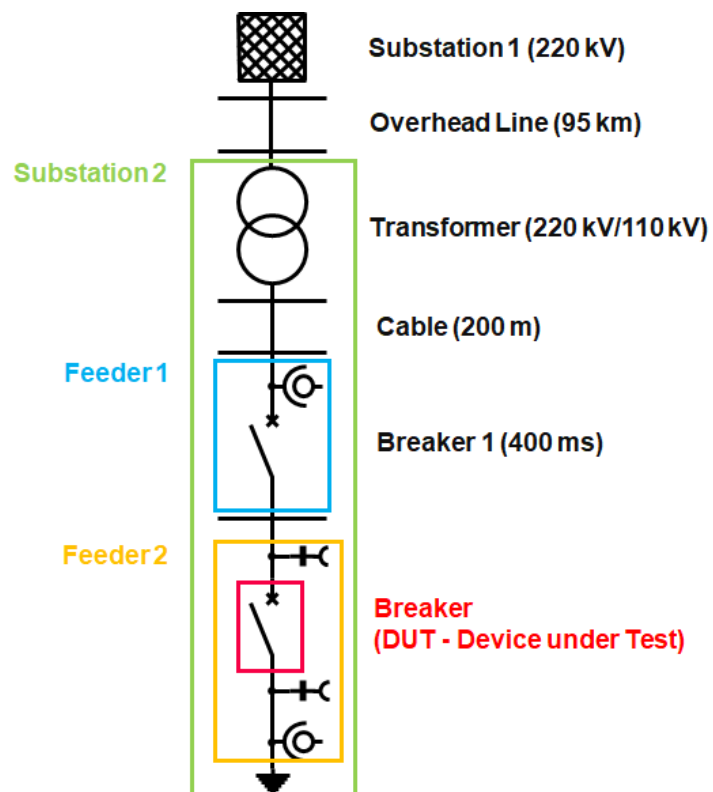


Figure 4.1.: Overview of the Measurement Setup

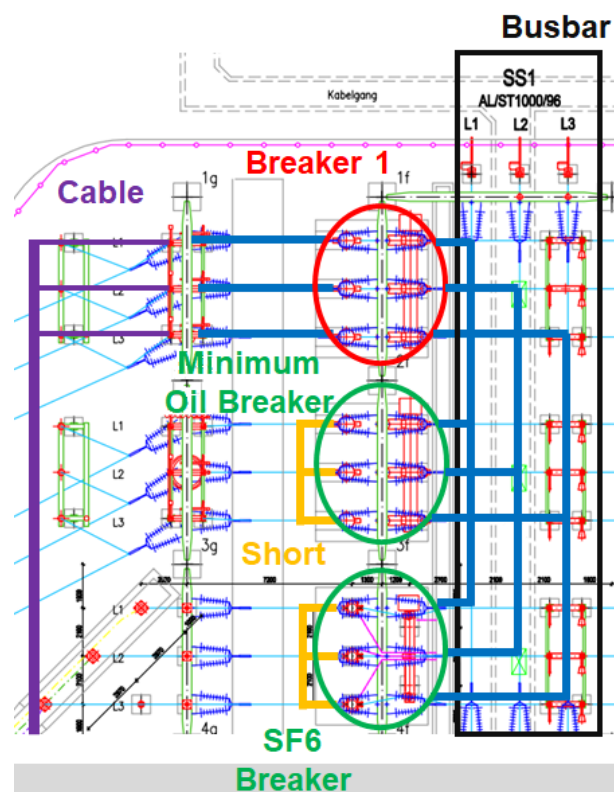


Figure 4.2.: Layout of the Measurement Area

4.2.3. Measurement Equipment and Short Circuit

The figure 4.3 shows how the short circuit was formed with three earthing sets at the end of the circuit breaker. Each phase is connected to earth and in this way a 3-pole short circuit is formed with earth contact. Furthermore, a combined transformer for voltage and current measurement is visible. This measuring device can detect overvoltages and short circuits. However, it is designed for the operating frequency of 50 Hz and is not suitable for measuring fast transient processes.

For this purpose, voltage dividers were installed before and after the circuit breaker under test, as shown in the figure 4.4. These consist of an ohmic-capacitive divider and satisfy the required sampling rate. The picture also shows a minimum oil circuit breaker with the typical V-shape.



Figure 4.3.: Minimum Oil Circuit Breakers - Combined Transformers (green) and the Earthing Set (yellow)



Figure 4.4.: Voltage Measurement Before and After the Circuit Breaker (red) via Ohmic-Capacitive Voltage Dividers (blue)

4.3. Measurement Results

4.3.1. SF6 Circuit Breaker

The following lines discuss the results of the measurement with the SF6 circuit breaker. In figure 4.5 are the measured voltages of two phases before the switch from the measurement. Here the short circuit was switched on and cleared by the circuit breaker after about 300 ms. The time results from the tripping time (200 ms) and the time the breaker needs to open and extinguish the arc. For this thesis the opening procedure is of particular interest.

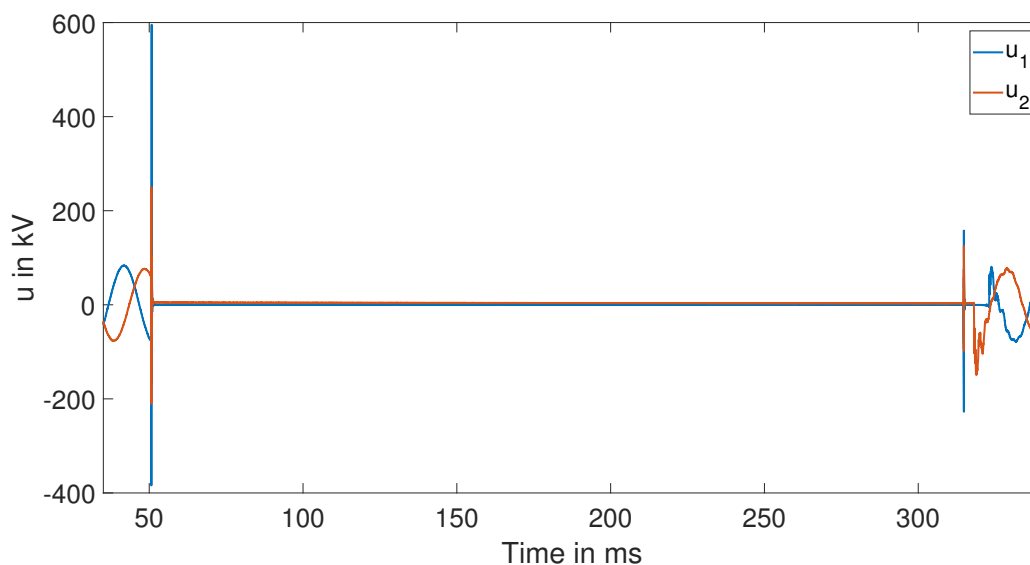


Figure 4.5.: Switching Voltages of SF6 breaker

4.3.2. Opening Process

The figure 4.6 shows an enlarged section of this opening process and various effects can be observed. At the beginning there is a high peak before the voltage comes back. This occurs because the dielectric strength cannot be recovered fast enough during the opening. This leads to a new breakdown of the spark gap called reignition and causes very fast transient processes.

Furthermore, two distinct transient frequencies are visible. This is a frequency of about 500 Hz and a faster one with about 5 kHz. These transients are strongly damped and do not occur after a quarter period anymore. Moreover, it can also be seen that the amplitude of the voltage is much higher at first than the amplitude of the nominal voltage. This occurs because the system is not symmetrical after the first pole opens and also the

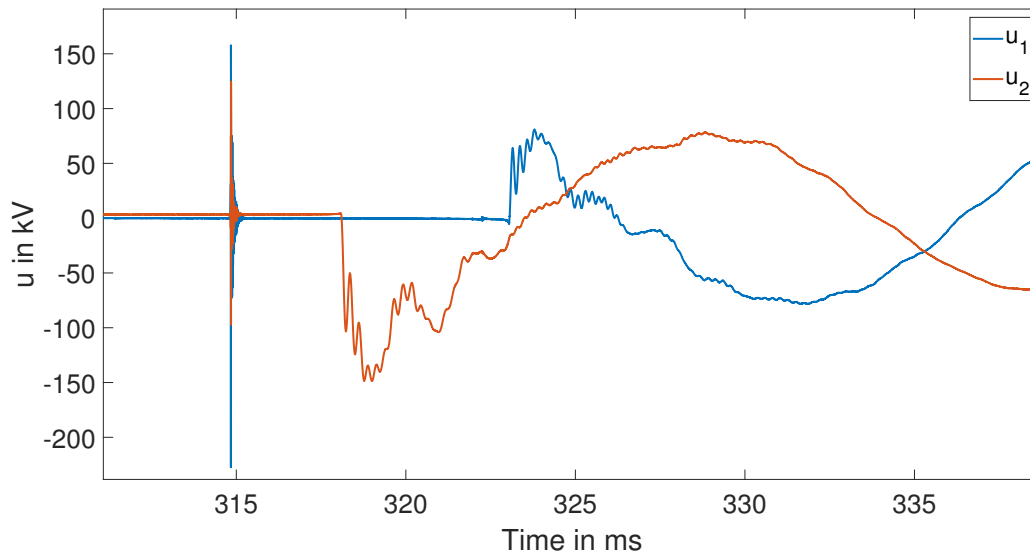


Figure 4.6.: Switching Voltages of Opening from SF6 Breaker

amplitudes of the transients add up. But it corresponds almost to the expected value of 1.5 times of the nominal amplitude.

4.3.3. Arc Voltage

If we zoom into the measured opening process and averages the measured values slightly, the arc voltage can be seen relatively clearly. The figure 4.7 shows it with the corresponding current in the same phase. It is recognizable how the arc voltage shows an extinguishing peak at the current zero crossing. The extinguishing of the arc was successful at this point, after which the transient recovery voltage occurs and no more current flows.

4.3.4. Reignition

At the beginning of the opening process a very high voltage peak is remarkable. This is because of the weak dielectric strength of the opened contacts, which is not yet given and breaks down. This triggers resonant circuits which lead to very high overvoltages. The figure 4.8 illustrates an enlargement of this phenomenon.

If the nominal voltage of the 110 kV power system is taken as a reference, the voltage peak results in a rise of about 2.5 p.u. (per unit) The frequency of this oscillation corresponds to a very fast transient with about 70 kHz.

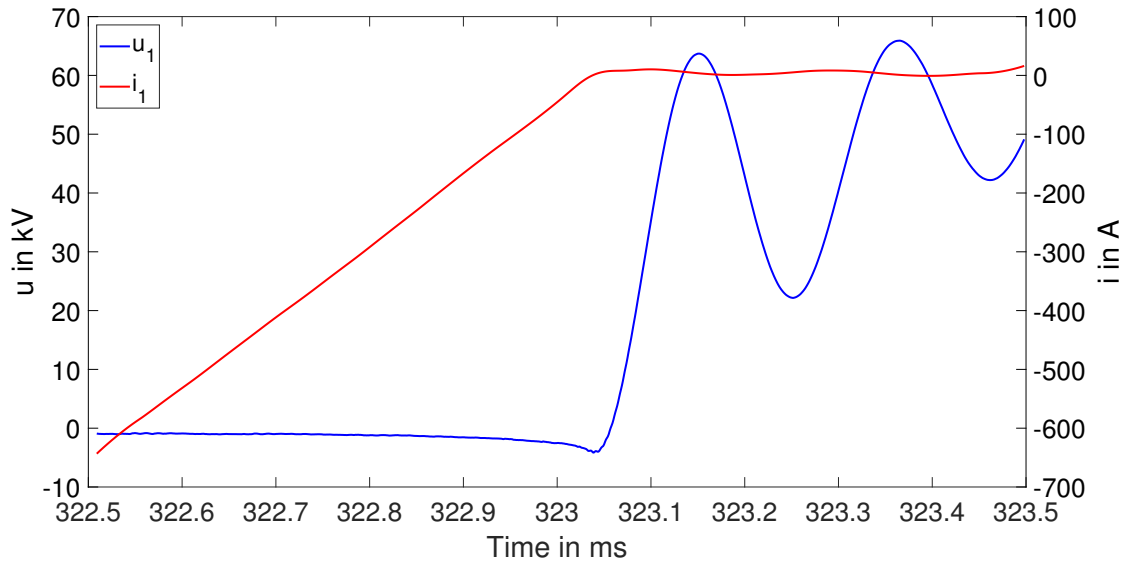


Figure 4.7.: Arc Voltage of Phase 1, with Corresponding Current

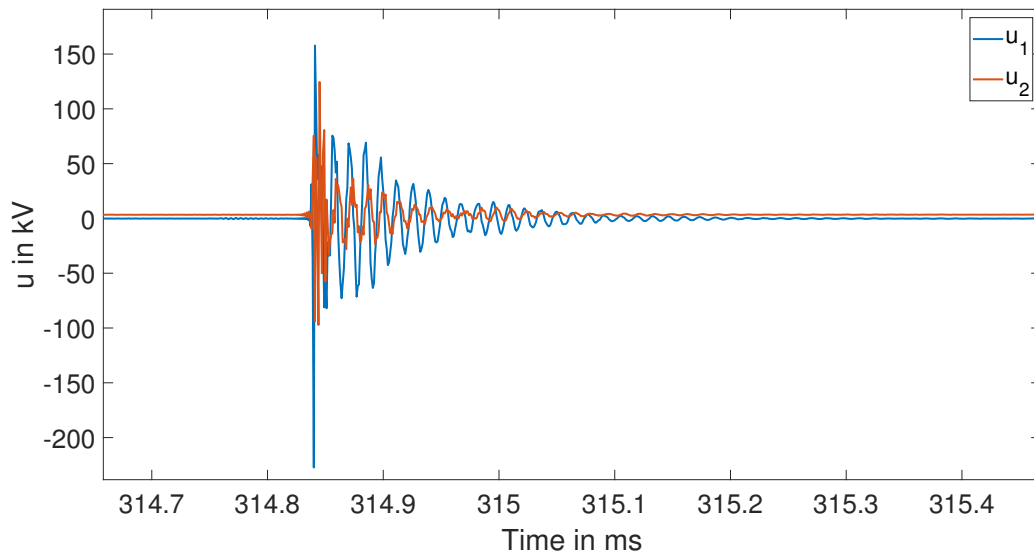


Figure 4.8.: Multiple Reignitions of SF6 Breaker

$$\hat{U}_{phase} = \sqrt{2} \cdot \frac{U_{nominal}}{\sqrt{3}} = \sqrt{2} \cdot \frac{110 \text{ kV}}{\sqrt{3}} = 90 \text{ kV} \quad (4.1)$$

$$\hat{u}_{peak} = \frac{\hat{U}_{peak}}{\hat{U}_{phase}} = \frac{230 \text{ kV}}{90 \text{ kV}} = 2.5 \text{ p.u.} \quad (4.2)$$

4.3.5. Fourier Transformation of Voltages

To determine other frequencies in the measured voltages of the circuit breaker, a FFT (Fast Fourier Transformation) was performed on both signals. This is represented in figure 4.9. The operating frequency voltage can be clearly recognized. The slow transient frequency is also indicated by a peak. The fast transient voltage is unfortunately very strongly attenuated, so that it is hardly visible in the frequency range. Furthermore, no more clear peaks can be recognized.

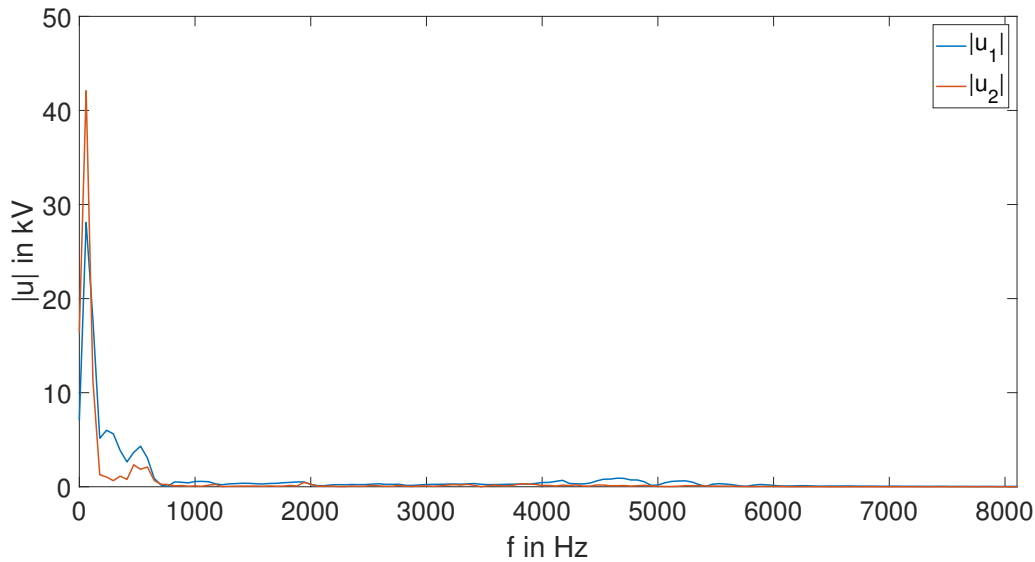


Figure 4.9.: FFT of the Measurement with the SF6 Circuit Breaker

4.3.6. Minimum Oil Circuit Breaker

The figure 4.10 shows the measured switching voltages for the opening with the minimum oil circuit breaker. Here three peaks are recognizable whereby the amplitudes are even above the one of the SF6 breaker. Furthermore, the amplitude height after the first extinguished pole is also much higher with about 200 kV.

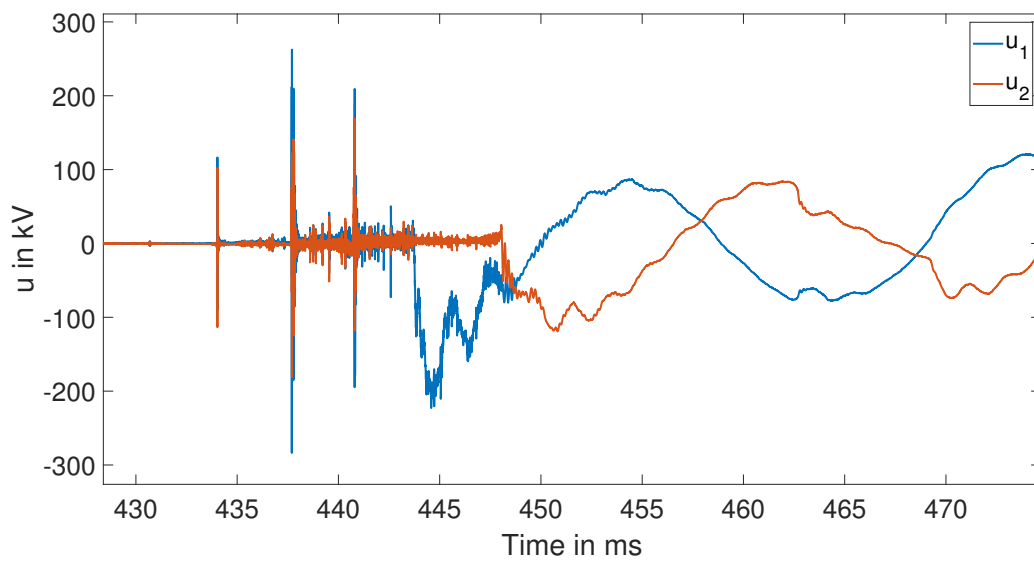


Figure 4.10.: Switching Voltages of Opening from Minimum Oil breaker

5. EMTP-Introduction

5.1. Simple Example

In this section the process of switching voltages should be showed based on a simple example. The figure 5.1 shows a resistor, inductance and capacitance connected in series. This circuit is supplied with an DC voltage source of 1 Volt. In the beginning the capacitor is shorted with the switch, but after 50 ms the switch opens.

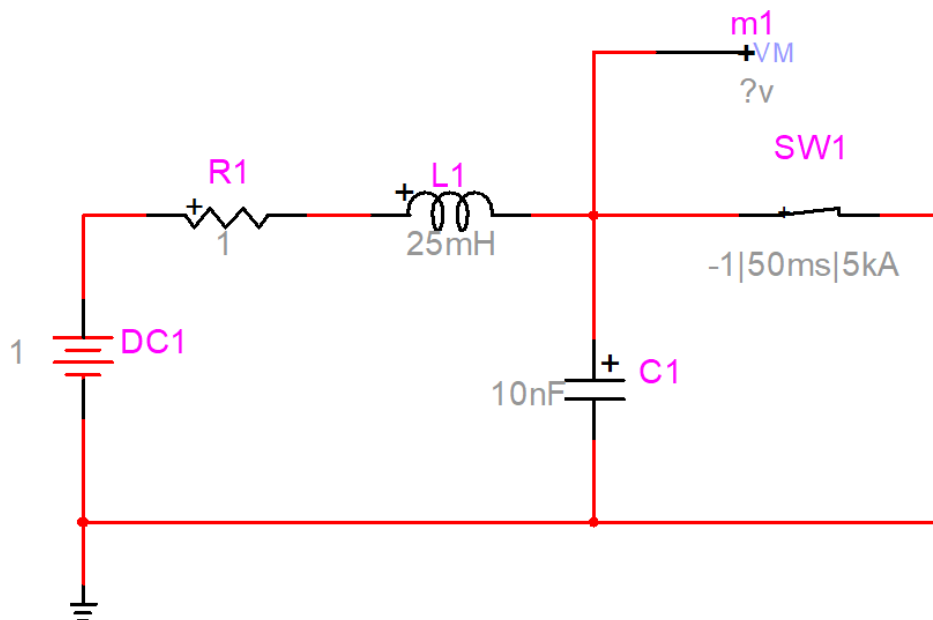


Figure 5.1.: Schematic of Simple Switching Circuit

The figure 5.2 shows the simulation result of this circuit. On the x-axis there is the time and on the y-axis is the voltage of the capacitor plotted.

At first the capacitor is shorted out by the switch and therefore the voltage is 0 Volt. The switch opens at 50 ms and the series resonance circuit was initiated. After 1 s the capacitor is in a steady state again and charged on the source voltage. In between there is a AC voltage with the eigenfrequency. By neglecting the resistance this f_g (resonance frequency) can be calculated with the inductance and capacitance. With the values of $L = 25 \text{ mH}$ and $C = 10 \text{ nF}$ this frequency is 10 kHz rounded.

$$f_g = \frac{1}{2\pi \cdot \sqrt{L \cdot C}} = \frac{1}{2\pi \cdot \sqrt{25 \text{ mH} \cdot 10 \text{ nF}}} \approx 10 \text{ kHz} \quad (5.1)$$

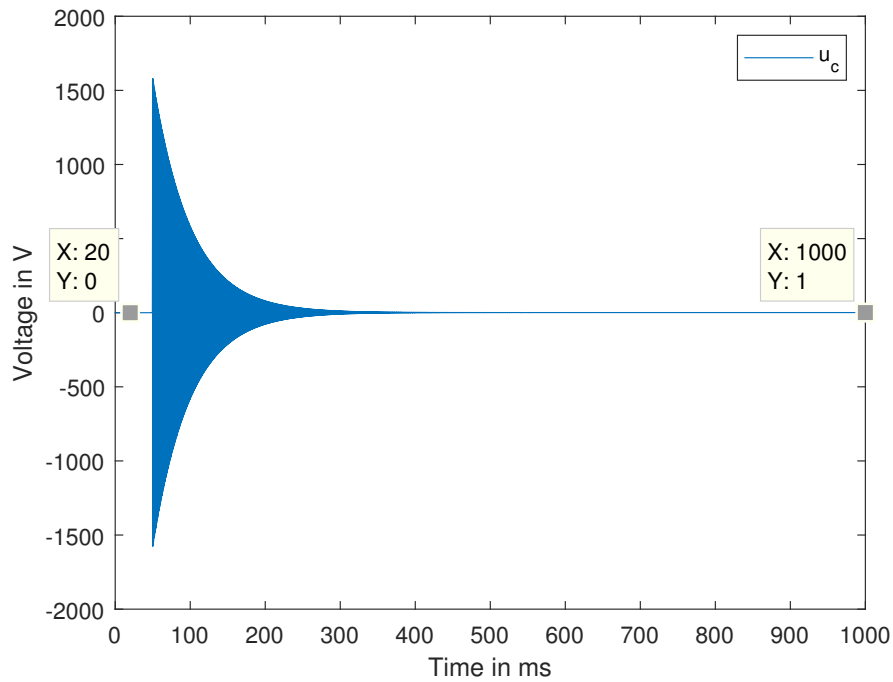


Figure 5.2.: Voltage at the Capacitor - Simple Example

The figure 5.3 shows an enlargement of the area from the AC voltage. With the measured period time the frequency can be calculated with the following equation and it shows that this measured frequency is equal to the calculated one before.

$$f_{meas} = \frac{1}{T} = \frac{1}{0.1 \text{ ms}} = 10 \text{ kHz} \quad (5.2)$$

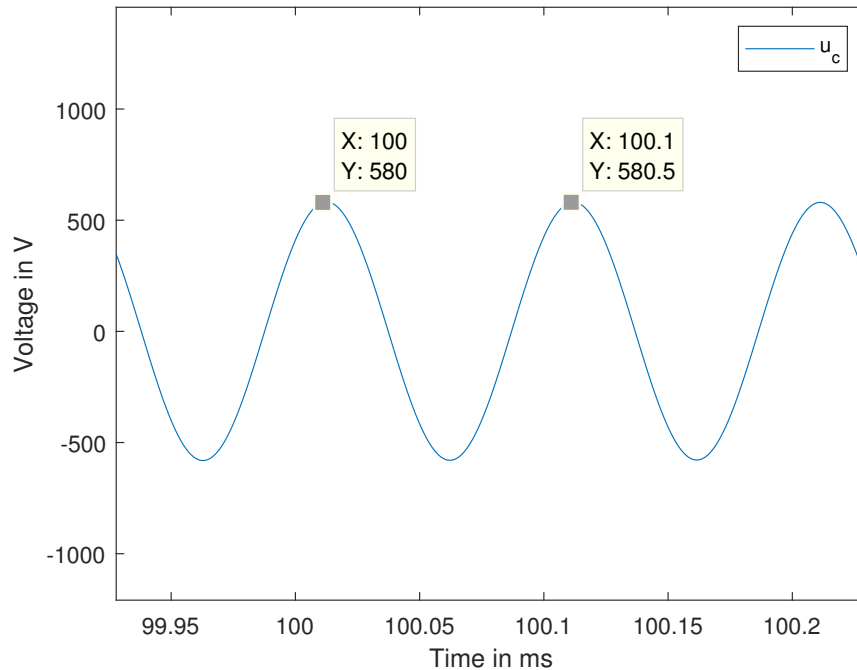


Figure 5.3.: Enlargement of the Resonance Frequency - Simple Example

5.2. Cable Models

The following pages will explain the usage of different cable models of the simulation program and the differences of each model will be evaluated. Therefore as a reference the cable NKT Cu 76/132kV 300mm² is used and the datasheet is attached in the appendix. For the application in the time-domain the CP (constant parameters) model, FDQ (frequency depending Q matrix) model and WB (wideband) model are interesting. The complexity increases from the CP model to the WB model.

5.2.1. CP Model

The CP model is the easiest model for cables because the parameters are assumed to be constant over all frequencies. But even there are more possibilities to enter the parameters. The least complicated one is if the parameters of the zero and positive (=negative) sequence are given. It is possible to enter the parameters in the three following ways:

- values per length unit R' , L' and C'
- resistance per length unit R' , the surge impedances Z_W and propagation speeds v
- resistance per length unit R' , the surge impedances Z_W and propagation delays τ

The second possibility is to build the model with the cable geometry. This option is

the only possibility to enter the parameters of the other models. Because of that, it was also done for the CP model to verify the results of the model before.

5.2.2. FDQ Model

The FDQ (Frequency Dependent Q matrix) underground cable model takes into account the frequency dependence of the cable parameters as well as the frequency dependence of the modal transformation matrix (T or Q). This model was specifically developed to model single core direct buried multiphase cables. To create the model the cable data with the geometry has to be used which is explained below.

5.2.3. WB Model

The WB (Wideband) model is the complexest line and cable modeling technique in EMTP (electromagnetic transient program). It represents the complete frequency dependence of parameters by calculation in the phase domain. The input of the parameters is as first step again with the cable data model. Then the WB fitter has to be used to generate the model file.

5.2.4. Cable Data - Geometry Input

In the cable data model it is possible to generate a cable model from the geometry. Therefore the main three different models CP, FDQ and WB can be chosen. In the next passages this generation will be done with the reference model. Figure 5.4 shows the main view of the model where the table at the top is about the location of the different cables. The figure 5.5 shows the designed placement of the cables at one level in the ground.

At the reference cable the values of the positive and zero sequence impedances are verified for the triangle placement (figure 5.6). Therefore the position of the three single conductor cables is also entered in this form. Each cable is a coaxial cable and has two conductors, which are the main conductor in the center and a shield around the inner isolation. The horizontal and vertical positions of the cables were calculated from the outer radius to get the triangle form.

$$height = \sqrt{(2 \cdot r_{out})^2 - r_{out}^2} = \sqrt{(2 \cdot 35.6 \text{ mm})^2 - (35.6 \text{ mm})^2} = 65.5 \text{ mm} \quad (5.3)$$

In the table at the bottom the user has to give in detail information about the conductor and insulator data. For the inner conductor the resistivity of copper with the diameter in the data sheet is used. The insulator is a 18 mm thick XPE (cross-linked polyethylene) layer. The insulator permittivity and insulator loss factor of XPE was taken.[11] After an insulation screen and a semi conductive water-blocking tape the shield wire begins. The outer radius was assumed to be higher than the calculated one with the effective screen area would be, because of a bulking factor. After that the cable ends with a non-conductive water-blocking tape, an APL (aluminium-polyethylene-laminated) sheath,

Geometrical and electrical data

Cable data						
Cable type		Single core	Number of cables			3
Cross-bond the Sheaths <input type="checkbox"/>						
	Cable Number	Number of conductors	Vertical Distance (m)	Horizontal Distance (m)	Outer Insulation Radius (m)	
1	1	2	0	0.0378	0.0378	
2	2	2	-0.0655	0	0.0378	
3	3	2	0	-0.0378	0.0378	

Conductor/Insulator data										
	Cable Number	Conductor Number	Inside Radius Rin [m]	Outside Radius Rout [m]	Resistivity Rho [Ohm-m]	Relative Permeability MUE	Insulator Relative Permeability MUE-IN	Insulator Relative Permittivity EPS-IN	Insulator Loss Factor LFCT-IN	Phase Number KPH
1	1	1	0	10.15E-3	1.68E-8	1	1	2.4	0.0004	1
2	1	2	30.35E-3	31.05E-3	1.68E-8	1	1	2.2	0.0002	2
3	2	1	0	10.15E-3	1.68E-8	1	1	2.4	0.0004	3
4	2	2	30.35E-3	31.05E-3	1.68E-8	1	1	2.2	0.0002	4
5	3	1	0	10.15E-3	1.68E-8	1	1	2.4	0.0004	5
6	3	2	30.35E-3	31.05E-3	1.68E-8	1	1	2.2	0.0002	6

Figure 5.4.: Cable Data Model - Input Parameters

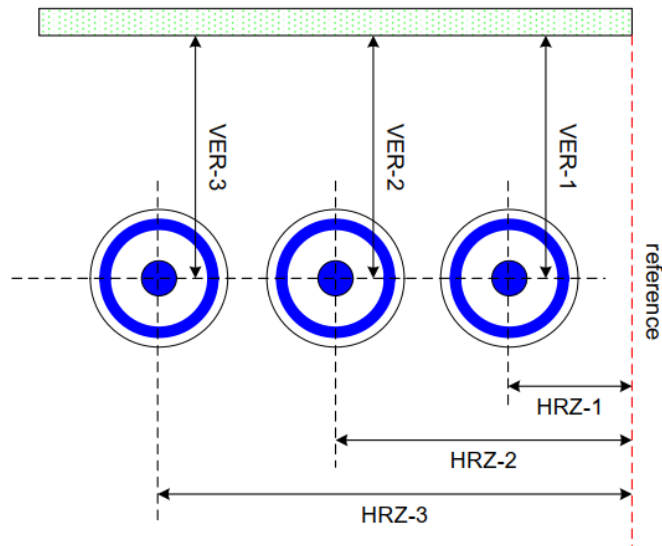


Figure 5.5.: Cable Data Model - General Geometry Input [8]

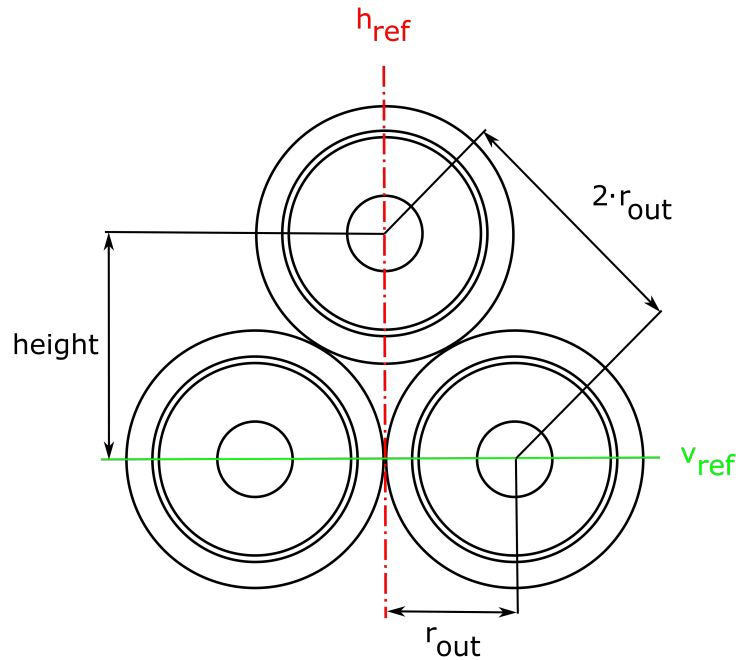


Figure 5.6.: Triangle Position Cable

a HDPE (high-density polyethylene) outer sheath and graphite coat. The insulation permittivity and insulator loss factor of HDPE to XPE vary slightly. [11]
 The KPH number gives information about the connections of the conductors at the model. All conductors with zero would be merged to one and connected to ground, but in this case it was chosen to connect the shield separately outside.

5.2.5. WB Fitter

The WB Fitter is used to generate a model for the WB model of the cable data or line data model. If the model does not converge it is possible to use various fitting techniques by activating different corrections. The figure 5.7 shows the fitting of the short reference cable.

5.2.6. Comparison of Cable Models

To compare the cable models a project with all model is made. Each cable model is connected to a voltage source and the positive and zero sequence impedance of the models were measured. Therefore the simulation option "frequency scan" from a frequency of 1 Hz to 100 kHz is used. Figure 5.8 shows the setup of one of this measurements.

Figure 5.9 is presenting the Bode plot of the positive sequence of each cable model. It can be seen that in the beginning the resistance makes a big influence, but with higher frequency the reactance becomes the main part.

Wideband line/cable data fitter function

Fitting convergence tolerance (%)

Passivity test

Cable model correction

Residue/Pole threshold for correction

DC correction

Apply grouping in propagation matrix fitting

Data input device name

Figure 5.7.: WB Fitter - Properties of Data Fitter

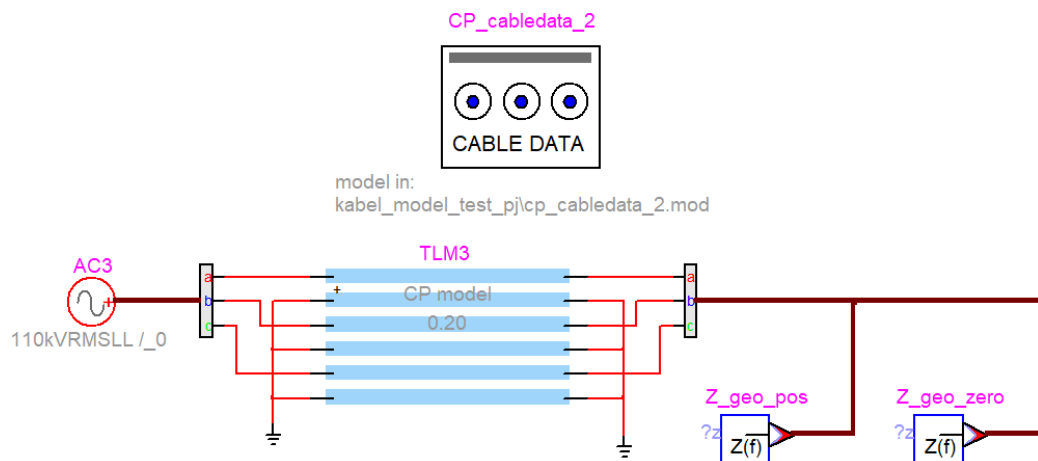


Figure 5.8.: Cable Model Setup

It is noticed that the CP model with entering the parameters manually Z_z is almost same as the one where the geometry Z_{geo} is used. Noticeable are that the FDQ (Z_{fdq}) and WB (Z_{wb}) models are also quite similar, but compared to the CP models there is a bigger gap especially at high frequencies.

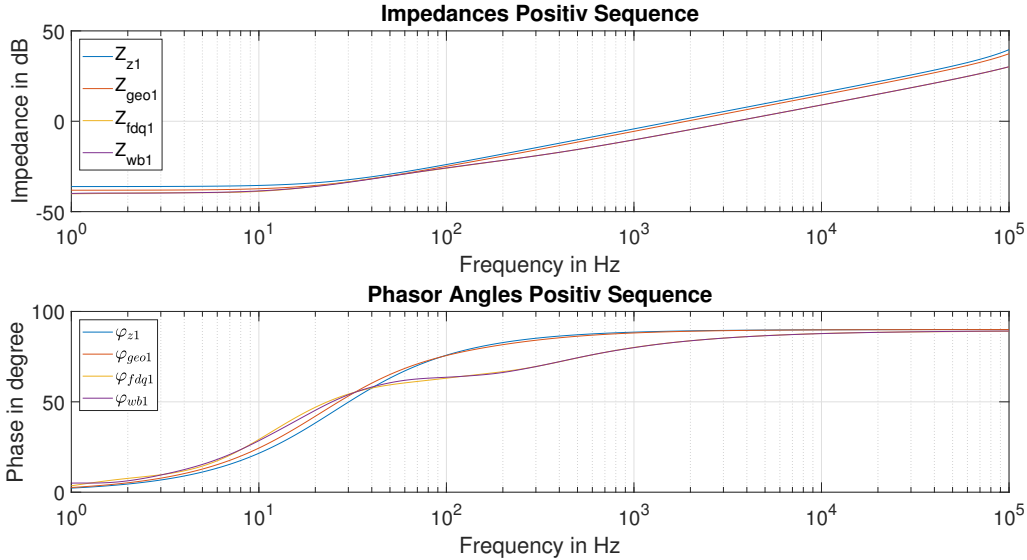


Figure 5.9.: Bode Plot of Positive Sequence referenced on $1e^{j0} \Omega$ - Cable models

For a better comparison the figure 5.10 and figure 5.11 show the positive sequence resistances and inductances of interest of each model. On the the x-axis the frequency is plotted logarithmic to show the operating frequency but also very high ones in a good way.

It can be seen that the resistance at the CP model with entered parameters is constant over all frequencies. The CP model with the geometric data suits this, but deviates slightly due to inaccuracies in the calculation at higher frequencies. Because the parameters of this model should be constant this error is the result of rounding errors where the angle is near to 90 degrees.

The frequency depended models consider the skin effect of the wire. That results to higher resistances at higher frequencies because the current flows only at the edge according the skin effect.

The inductance of the CP models is again quite similar and constant for the most part. Because the inductance also depends on the frequency, the frequency depending models show a decrease. This is due to the decrease of the internal inductance.

For the purpose of completeness, figure 5.12 shows the Bode plot of the zero sequence impedance. It can be seen that the angle approaches 90 degrees and the impedance

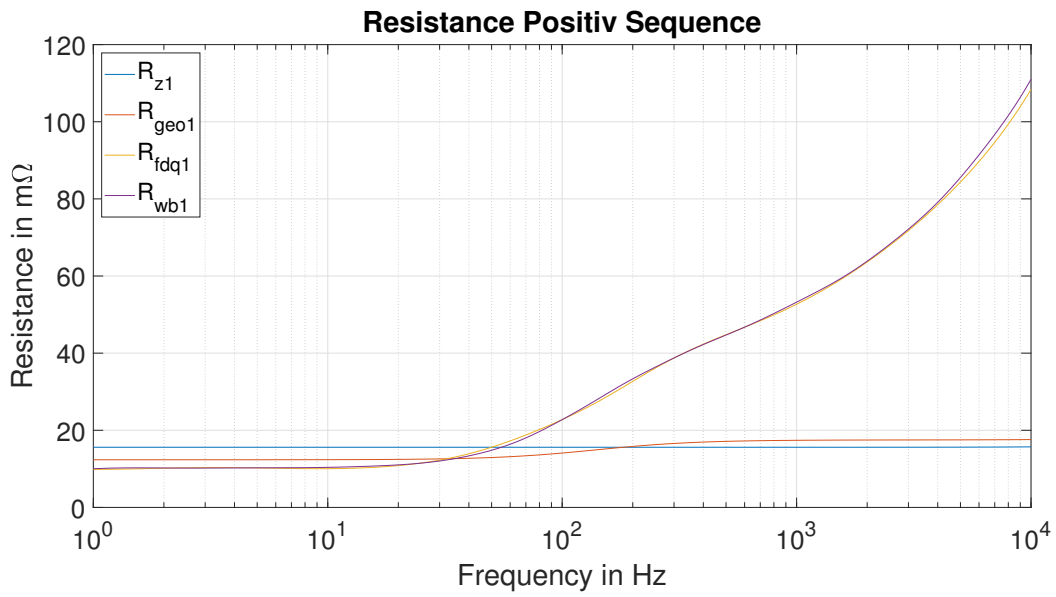


Figure 5.10.: Resistances of different Cable models

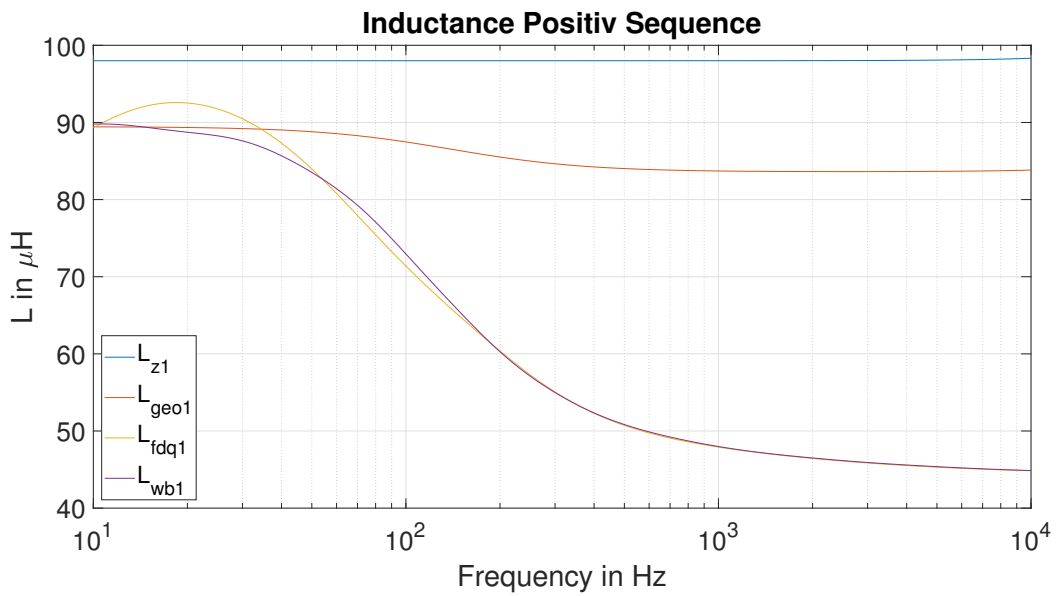


Figure 5.11.: Inductances of different Cable Models

increases with 20 dB per decade.

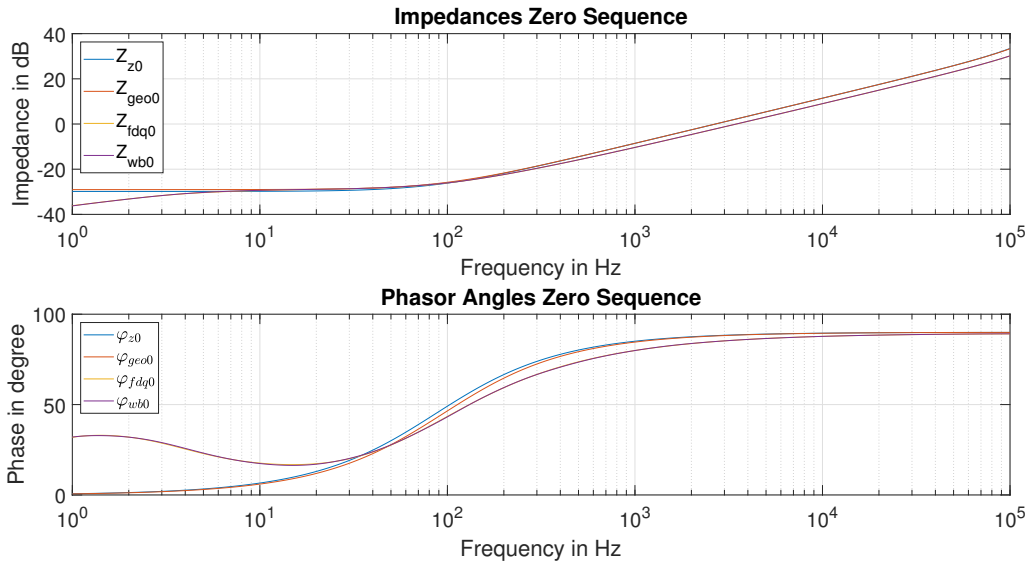


Figure 5.12.: Bode Plot of Zero Sequence referenced on $1e^{j0} \Omega$ - Cable Models

5.2.7. Influence of the Shield Earthing

Until now it was assumed that the shielding of the cables was connected to earth at both ends. In this chapter we will now discuss if this is not the case for at least one end. For the simulation, an impedance measurement of the constant parameters cable model for the zero and positive sequence impedance over different frequencies is done as before. As can be seen in the figure 5.13, the cable ends are not always grounded.

Figures 5.14 and 5.15 now show the dependency of the positive and zero sequence impedance over the frequency. It can be seen that the model with open ends has clearly pronounced peaks. Peaks also occur in models where one side is not grounded. It has been found that the peaks occur at periodic intervals of twice the frequency of the first peak. If the shields are grounded at both sides there are no peaks in this frequency range.

This has to do with the propagation time in the zero sequence system. Unfortunately, due to the complex coupling of the 6 different conductors, no analytical solution could be found. However, this experiment shows that due to certain couplings several resonance frequencies can appear in the model. It is worth mentioning that in this case they appear at a very high frequency, whereby these are strongly damped in the system and will not effect the results.

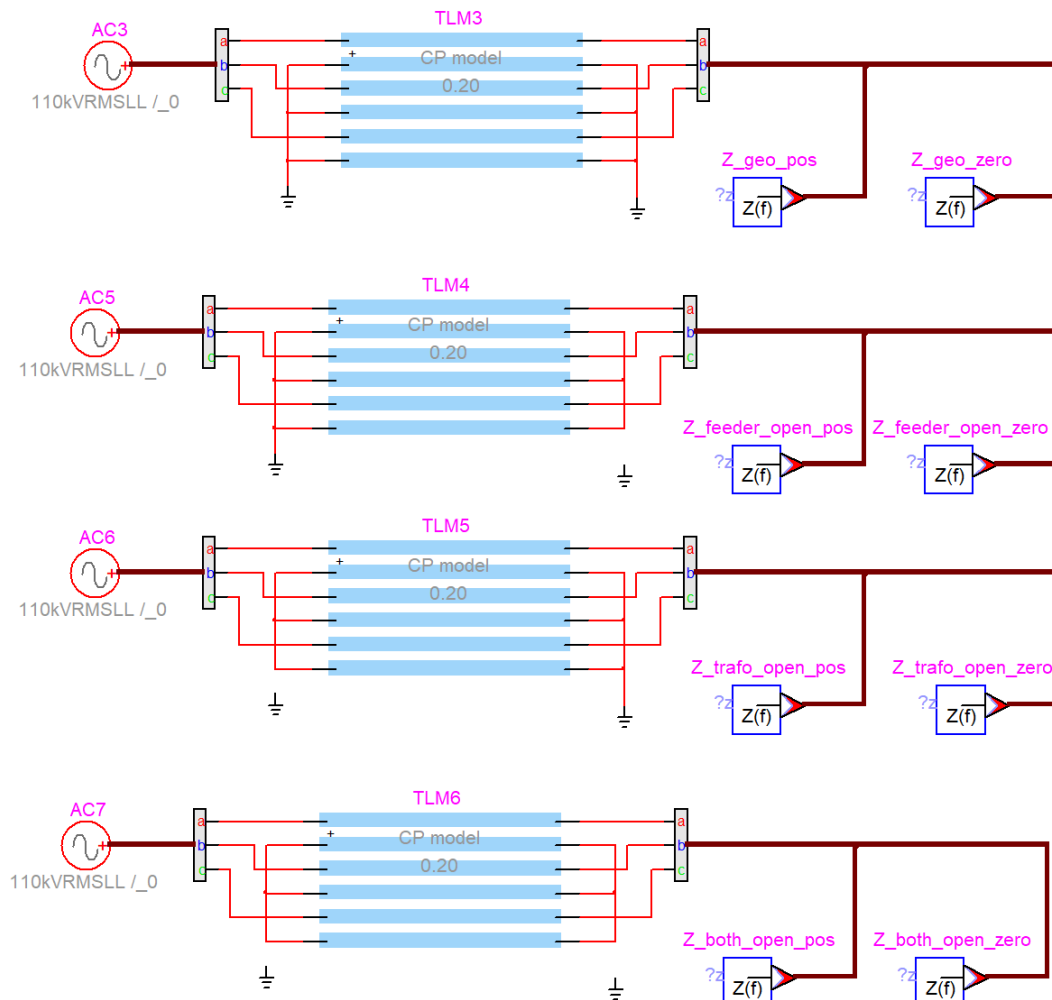


Figure 5.13.: Measurement Setup for different Shielding

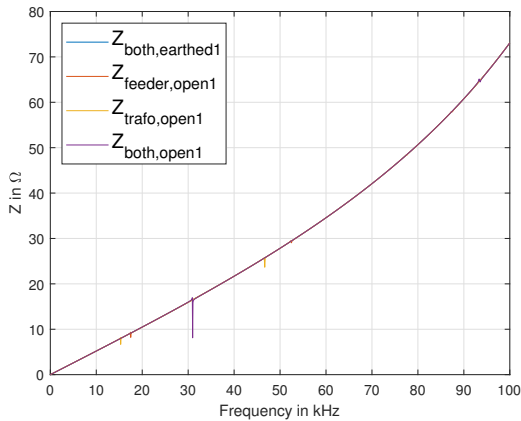


Figure 5.14.: Positive Sequence Impedance of different Connections of the Shield

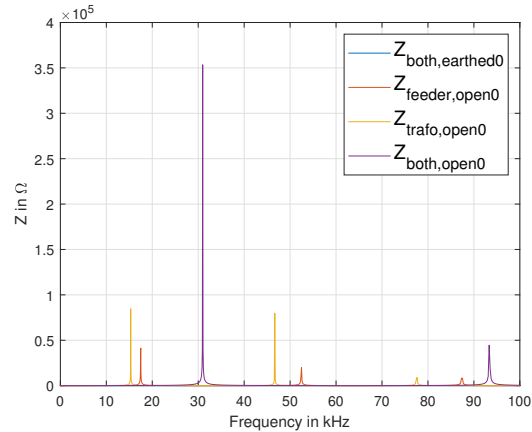


Figure 5.15.: Zero Sequence Impedance of different Connections of the Shield

5.3. Line Models

Figure 5.16 shows an overview of all possible line models in EMTP. For the time-domain simulation the CP, FD (frequency depending) and WB models are of interest. The difference of the frequency depended models is that in the WB model the modelling is in the phase-domain and therefore also the transformation matrix is frequency depended. This model is as a consequence the most sophisticated and most accurate one.

Overview of Line Models

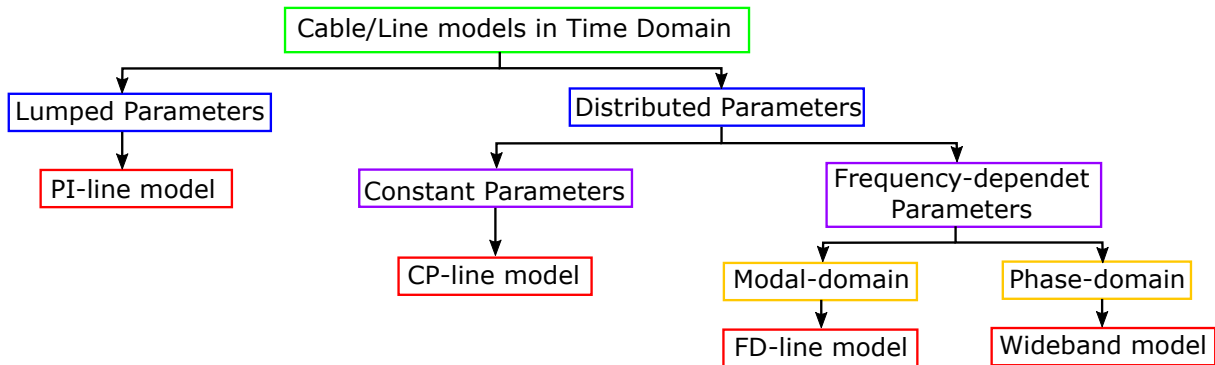


Figure 5.16.: Overview of Line Models

As for the cable models there are more possibilities to model the line. For the CP line model the parameters can entered again directly if the data of the positive and zero sequences are given. As a second option it is again possible to enter the data with the geometry. Furthermore, in the line data model it is also possible to rebuild the line if the

conductor data are given for a specific frequency. For the frequency depending models the rebuild and the geometry option can be used. The following lines explain and compare the mentioned input options using the reference overhead line. The datasheet can be found in the appendix.

5.3.1. Line Rebuild

This input option enables the simulation of an overhead line on the basis of the parameters it has for a certain frequency. The line parameters per unit of length for the positive and zero sequence must be known. Furthermore, the DC resistance is required of the conductor. The figure 5.17 shows the known values for the reference overhead line. If these data are known, this method is a practical way to build the CP model and the frequency dependent models. Here the parameters for other frequencies are calculated in the background.

Geometrical and electrical data

Module ▾

Units ▾

Input option ▾

Conductor Data	
Number of Phases	3
R zero sequence [Ohm/km]	0.233
L zero sequence [mH/km]	3.393
G zero sequence [S/km]	0.05E-6
C zero sequence [microF/km]	5.549E-3
R positive sequence [Ohm/km]	0.084
L positive sequence [mH/km]	1.321
G zero sequence [S/km]	0.05E-6
C positive sequence [microF/km]	8.946E-3
Frequency [Hz]	50
DC resistance [Ohm/km]	0.084

Figure 5.17.: Rebuild Input Data - Line Model

5.3.2. Geometry Input

If the line parameters are not known but the overhead line geometry is known, this input option can be used. The figure 5.18 shows the necessary inputs for the reference overhead line, if only one system is considered.

The upper area shows the input of the conductor resistances and their position in relation

to the axis of symmetry of the mast. If zero is entered for a phase number, this line is assumed to be an earth wire.

Geometrical and electrical data

Module: Line Model
 Units: Metric
 Input option: Standard Conductor data
[Use Database](#)

Conductor Data
 Number of conductors (wires): 4

Wire	Phase Number	DC resistance [Ohm/km]	Outside diameter [cm]	Horizontal distance [m]	Vertical Height at tower [m]	Vertical Height at Midspan [m]
1	1	0.084	2.79	-5	33.15	33.15
2	2	0.084	2.79	-7	26.48	26.48
3	3	0.084	2.79	-5.5	20.30	20.30
4	0	0.233	1.65	0	41.65	41.65

Additional data for Wire 1

Skin effect correction

Thick/Diam: 0.25
 None
 Solid conductor
 Galloway Wedepohl

Bundled Conductor

Relative permeability: 1

Figure 5.18.: Geometry Input Data - Line Model with one System

In the lower area the skin factor correction can be taken into account. In this case the Thick/Diam option is selected, where the thickness of the aluminium conductor is divided by the diameter of the entire conductor. This factor lies between 0 and 0.5, where 0.5 corresponds to a solid conductor. Figure 5.19 shows which thickness and diameter should be used in more detail.

5.3.3. Different Geometries

Since the overhead line that was used has two systems and an earth wire, the model could be realized in different ways for the geometry input. For the measurements only one system was used and for the other one there are several possibilities to model it:

- Second system not existing
- Second system opened

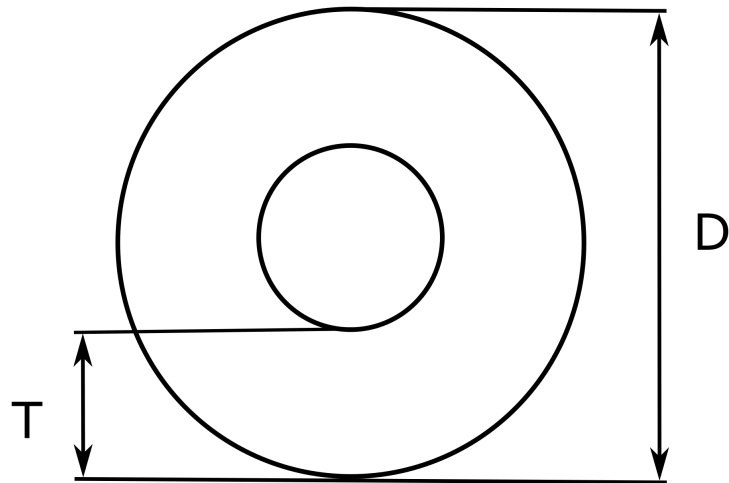


Figure 5.19.: Line Model - Skin Effect Correction

- Second system earthed
- Second system loaded

These possibilities were realized in EMTP and investigated for positive and zero sequence impedance. It turned out that the positive sequence is hardly influenced by this second system. But the zero sequence system depends on this input especially at very high frequencies.

In the overhead line data sheet the parameters for one system, two systems and one system, where the other one is earthed, are given. This allows to use the geometry input with one system for the comparison with the rebuild function input.

5.3.4. Comparison of Line Models

As there are also different input options for the line model and frequency dependent and constant parameter models, these are compared in the following lines. This is the input with the parameters from the data sheet Z_z , the input using the geometry Z_{geo} and the rebuild function $Z_{rebuild}$ for constant parameter model. Furthermore, the frequency dependent Z_{fd} and the wideband model Z_{wb} were also compared. As in chapter 5.2.6 for the comparison of the cable models the positive and zero sequence impedances were simulated by an impedance measurement. The Frequency Scan option was used again for this purpose, whereby the impedance measurement was made for all set frequencies.

Figure 5.21 shows the simulated Bode plot for the positive sequence impedance of the different line models. It can be seen that at higher frequencies the wave effects cannot be neglected. Especially the high peaks are noticeable. These occur due to resonant frequencies, whereby the short circuit created by the measurement setup is measured as

an open circuit.

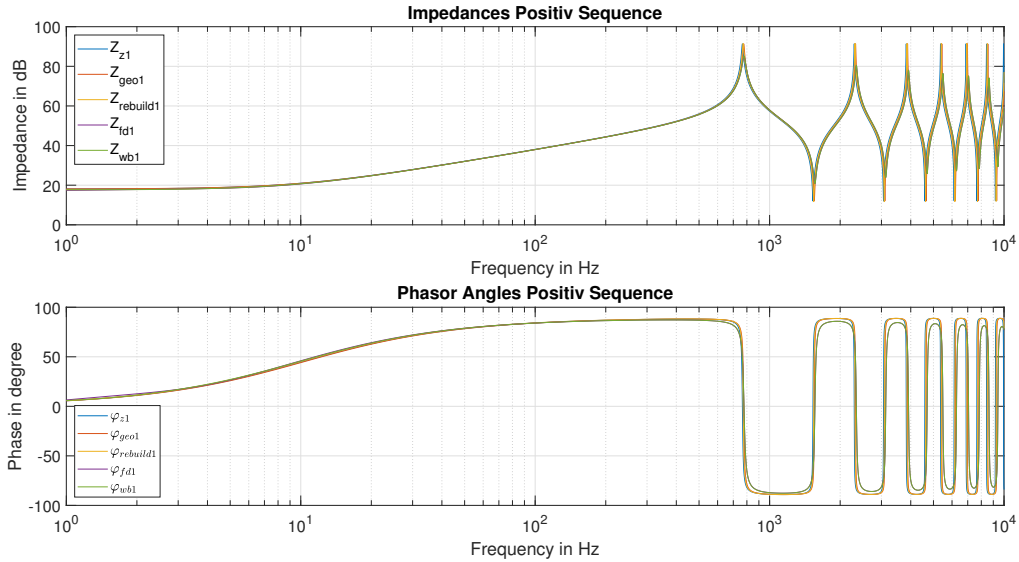


Figure 5.20.: Bode Plot of Positive Sequence referenced on $1e^{j0} \Omega$ - Line Models

On closer inspection in the higher frequency range, an attenuation of the peaks can be seen in the frequency dependent models. This is mainly due to the higher attenuation caused by the increased resistance value. However, the models are the same at the operating frequency of 50 Hz and for all input options quite similar.

For completion, figure 5.21 shows the Bode plot for the zero sequence impedances. It can be seen that the frequency dependence plays a higher role.

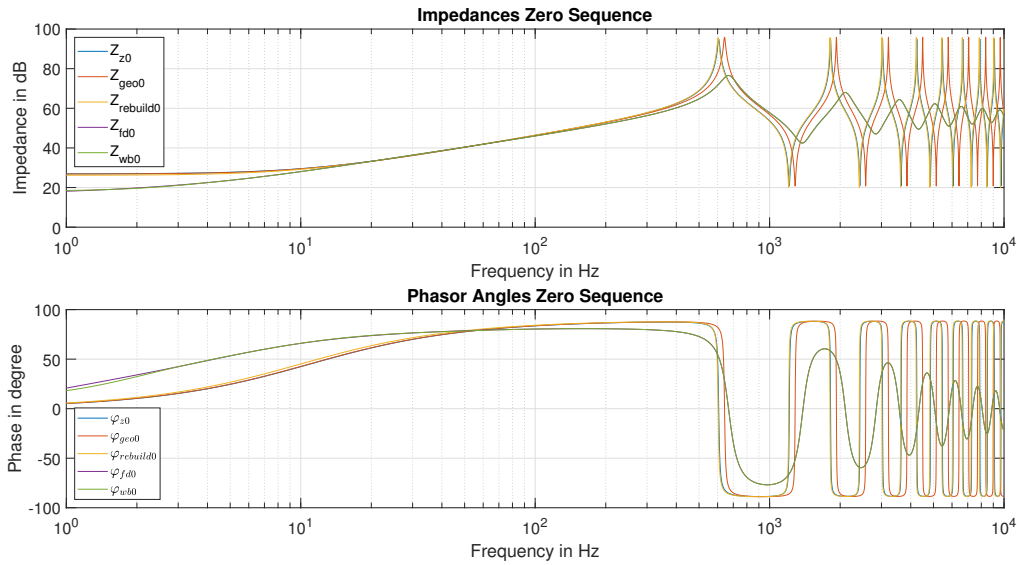


Figure 5.21.: Bode Plot of Zero Sequence referenced on $1e^{j0} \Omega$ - Line Models

5.4. Busbar Model

The connection from the cable to the test circuit breaker is made through a feeder and a busbar. This section is modelled as a line model using geometry, assuming the mean distances. The resistances and capacitances of components like different switches and measurement instruments are neglected. The figure 5.22 shows the geometry used for this and in figure 5.23 there are the corresponded input parameters.

The cross sections of the aluminium-steel conductor can also be found for the skin-effect correction. AL/ST 1000/96 stands for a effective cross section of 1000 mm^2 of aluminium and 96 mm^2 of steel in the center. The length of this element is estimated to be 40 meters and the frequency dependent models and the CP model are used here again. Compared to the overhead line model this geometry results to slightly different results because of the higher cross sections and the lower height to the ground.

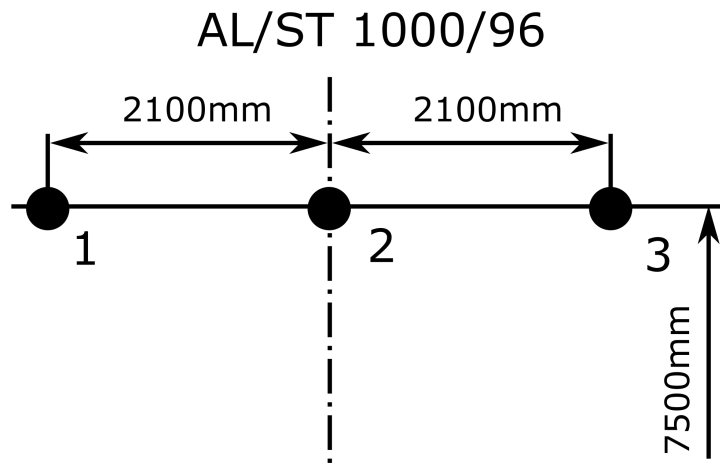


Figure 5.22.: Geometry Simplified Connection through Feeder 1 and Busbar

Geometrical and electrical data

Module: Line Model
 Units: Metric
 Input option: Standard Conductor data
[Use Database](#)

Conductor Data
 Number of conductors (wires): 3

Wire	Phase Number	DC resistance [Ohm/km]	Outside diameter [cm]	Horizontal distance [m]	Vertical Height at tower [m]	Vertical Height at Midspan [m]
1	1	0.0277	4.3	-2.1	7.5	7.5
2	2	0.0277	4.3	0	7.5	7.5
3	3	0.0277	4.3	2.1	7.5	7.5

Additional data for Wire 1

Skin effect correction

Thick/Diam: 0.36
 None
 Solid conductor
 Galloway Wedepohl

Bundled Conductor

Relative permeability: 1

Figure 5.23.: Geometry Input Data - Simplified Connection through Feeder 1 and Busbar

5.5. Transformer Model

The following figure 5.24 shows the equivalent circuit diagram of a transformer as it is implemented in EMTP for each phase individually. Here the leakage inductance of the primary winding and its ohmic resistance is located in the primary side. The same is on the secondary side for the secondary winding. In the middle there is an ideal transformer which represents the voltage ratio of the two sides.

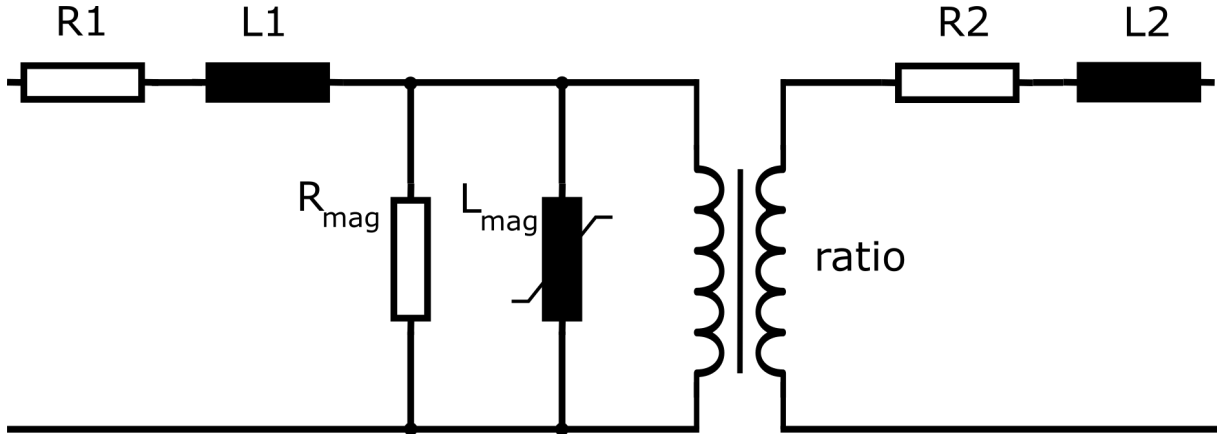


Figure 5.24.: Transformer Equivalent Circuit Diagram

To calculate the reactances and resistances of the transformer in per unit, the short-circuit voltage u_s , the short-circuit power P_s and the rated power S_r is needed. It can be seen that the resistance compared to the reactance is very small and therefore is usually neglected for big transformers. The division of these values between the primary and secondary circuit are usually 50:50 in per unit values. For the calculation the impedances must be calculated using the voltage ratio.

$$u_R = \frac{P_s}{S_r} = \frac{475 \text{ kVA}}{220 \text{ MVA}} = 0.00216 \text{ p.u.} \quad (5.4)$$

$$u_X = \sqrt{u_s^2 - u_R^2} = \sqrt{0.135^2 - 0.00216^2} = 0.13498 \text{ p.u.} \quad (5.5)$$

The resistance parallel to the primary side R_{mag} is called magnetizing resistance and represents the iron losses of the transformer. It is calculated by the no load power loss $P_{\text{no load}}$ as shown in the following equation. Parallel to this resistance is the magnetizing inductance L_{mag} . Due to saturation effects this component changes its value and is therefore not constant. This non-linear behaviour can be entered with the magnetic flux and the current or can be calculated via the current and voltage behaviour.

The magnetization resistance is calculated from the no-load losses and the nominal primary voltage. [11] To get the value in per unit values it has to be divided by the nominal

impedance. It can be seen that this resistance is very high and also sometimes neglected.

$$R_{mag} = \frac{U_r^2}{P_{noload}} = \frac{(220 \text{ kV})^2}{76 \text{ kW}} = 636.8 \text{ k}\Omega \quad (5.6)$$

$$R_{r,pu} = \frac{U_r^2}{S_r} = \frac{(220 \text{ kV})^2}{220 \text{ MVA}} = 220 \Omega \quad (5.7)$$

$$R_{mag,pu} = \frac{R_{mag}}{R_{r,pu}} = \frac{636.8 \text{ k}\Omega}{220 \Omega} = 2895 \text{ p.u.} \quad (5.8)$$

All calculated input parameters are shown in figure 5.25. Here a YGyg0 transformer is used to transform from the 220 kV to the 110 kV voltage level. The primary side is the transmission network which is solidly grounded. The secondary side is operated as resonant grounded neutral system, whereby the Peterson coil can be switched on or off.

3-phase transformer, 3 separate 1-phase units

Basic data

Connection Type

Nominal power MVA

Nominal frequency Hz

Winding 1 voltage kV RMSLL

Winding 2 voltage kV RMSLL

Winding R pu

Winding X pu

Winding impedance on winding 1

Magnetization data

Current-Flux units

	Current magnitude (pu)	Flux (pu)
1	.002	1
2	.01	1.075
3	.025	1.15
4	.05	1.2
5	.1	1.23
6	2.	1.72
7		
8		

Magnetization resistance pu

Exclude magnetization branch model

Figure 5.25.: Transformer Model Input Parameters

5.6. Peterson Coil

The following table has the most important parameters of the Peterson coil which was placed at the substation. With the rated power S_{rated} and rated voltage U_{rated} the rated reactance X_{rated} with the inductance L_{rated} can be calculated.

Table 5.1.: Parameters Peterson Coil

rated power	25403 kVA
rated voltage	$110/\sqrt{3}$ kV
rated current	400 A
current control range	40-400 A
rated frequency	50 Hz

$$X_{\text{rated}} = \frac{U_{\text{rated}}^2}{S_{\text{rated}}} = \frac{\left(\frac{110\text{kV}}{\sqrt{3}}\right)^2}{25403 \text{ kVA}} = 158.8 \Omega \quad (5.9)$$

$$L_{\text{rated}} = \frac{X_{\text{rated}}}{2\pi \cdot f} = \frac{158.8 \Omega}{2\pi \cdot 50 \text{ Hz}} = 505.4 \text{ mH} \quad (5.10)$$

It is possible to control the amount of windings to change the current range. That leads to a range of reactance rounded from 160Ω to $1,6 \text{ k}\Omega$ or for the inductance from 0.5 H to 5 H . Unfortunately the settings were not documented. However, it is expected that the coil was not in use for this experiments. In normal operation the coil is controlled in a way, that the whole network is slightly overcompensated.

$$X = \frac{U_{\text{rated}}}{I} = \frac{\frac{110\text{kV}}{\sqrt{3}}}{40 - 400 \text{ A}} \approx 1600 - 160 \Omega \quad (5.11)$$

$$L = \frac{X}{2\pi \cdot f} = \frac{1600 - 160 \Omega}{2\pi \cdot 50 \text{ Hz}} \approx 5 - 0.5 \text{ H} \quad (5.12)$$

5.7. Voltage Divider

For the measurement of the fast transient voltages, specially installed voltage dividers were used. These are ohm-capacitive voltage dividers with a very fast sampling rate of 1 mega-samples per second.

The figure 5.26 shows the structure of such a voltage divider with the corresponding measuring circuit. For the measurement the termination of the cable with the appropriate terminating impedance must also be taken into account. For the modelling of these components in EMTP the RC divider setup with R_p , R_s , C_p , C_s and a simplification, where only the small capacitance C_p is used, has been considered.

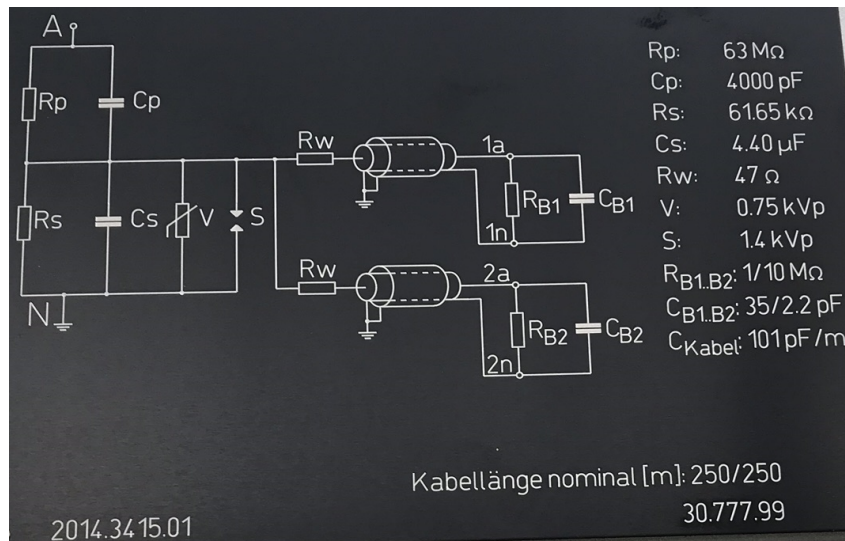


Figure 5.26.: Voltage Divider Nameplate

5.8. Switch Models

5.8.1. Ideal Breaker

First, the circuit breaker is modelled as an ideal switch. Here the closing and opening time can be selected. For this work the opening process is simulated, whereby the switch was closed in the steady state. For this, -1 must be entered for t_{close} . After a certain time the circuit breaker should open. The third parameter I_{margin} specifies the chopping current. The breaker opens if $t > t_{open}$ and the current is less than I_{margin} . If I_{margin} is set to 0, switching takes place at the current zero crossing. The figure 5.27 shows this three input parameters of an ideal breaker.

	Phase A	Phase B	Phase C	
t_{close}	-1	-1	-1	s
t_{open}	10	10	10	ms
I_{margin}	0	0	0	A
<input checked="" type="checkbox"/> balanced				
Never Open		Never Close		Closed in steady-state
Set closing time to 0				

Figure 5.27.: Ideal Breaker Settings

5.8.2. Breaker for TRV

EMTP offers a circuit breaker for the use of transient recover voltages. Here, the rated transient recovery voltage envelope can be added in further functions due to different

standards. After simulation it can then be determined whether the results are within the required range of the recovering voltage. Furthermore, the occurrence of restrikes and reignition can be added. Since stray capacitances also exist in a circuit breaker, they can also be included in this model. The figure 5.28 shows the possible input parameters for this model.

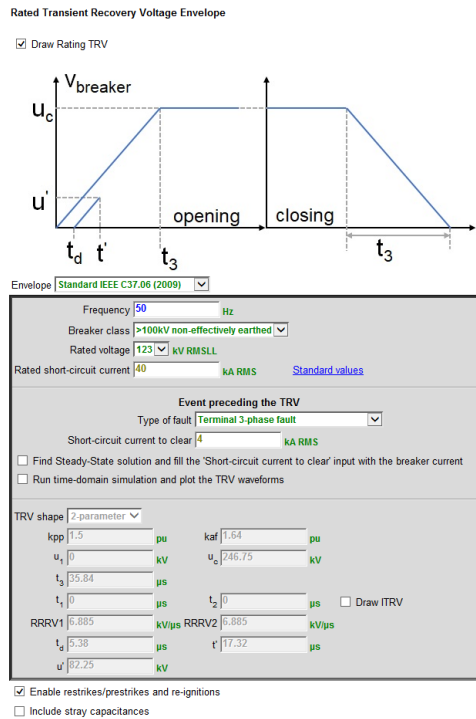


Figure 5.28.: Settings for Breaker for TRV

6. EMTP-Results

6.1. Simulation Model

To simulate the measured voltage, the complete system has to be modelled in EMTP. For this purpose the used elements have already been partially examined in detail in chapter 5. Figure 6.1 shows the complete simulation setup.

The complete model consists of one 3 phase voltage source, where this source with the impedance shall represent substation 1 and the grid. This source is connected with a 220 kV overhead line to the substation 2. The voltage is then transformed to 110 kV by the transformer and a cable is used to supply the circuit breaker via a feeder. After the circuit breaker the 3-pole short circuit is connected. Furthermore, the voltage dividers for measuring the voltage before and after the circuit breaker can be seen. At the set marker m1 the voltage can be plotted.

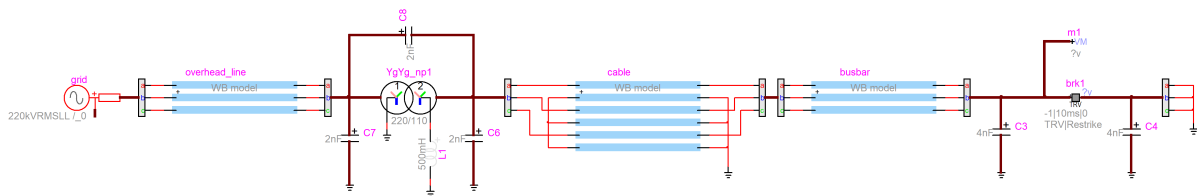


Figure 6.1.: Complete Simulation Setup

6.2. Simulation Results

6.2.1. Switching Voltages

Figure 6.2 shows the simulated voltages at the measuring point before the circuit breaker. The transient recovery voltage after the short circuit has been cleared, is clearly visible. Two distinct transient voltages can be detected. Over time, these are strongly attenuated and the operating frequency voltage remains. A voltage rise after the first pole-to-clear is also clearly visible.

The transient voltages contain of a slower one with about 645 Hz and a faster one with about 5.88 kHz. It was found that the slower one depends on the grid and the faster one

mainly on the transformer and the cable. The influence of the different parameters will be discussed more in detail in the Sensitivity Analysis 6.3.

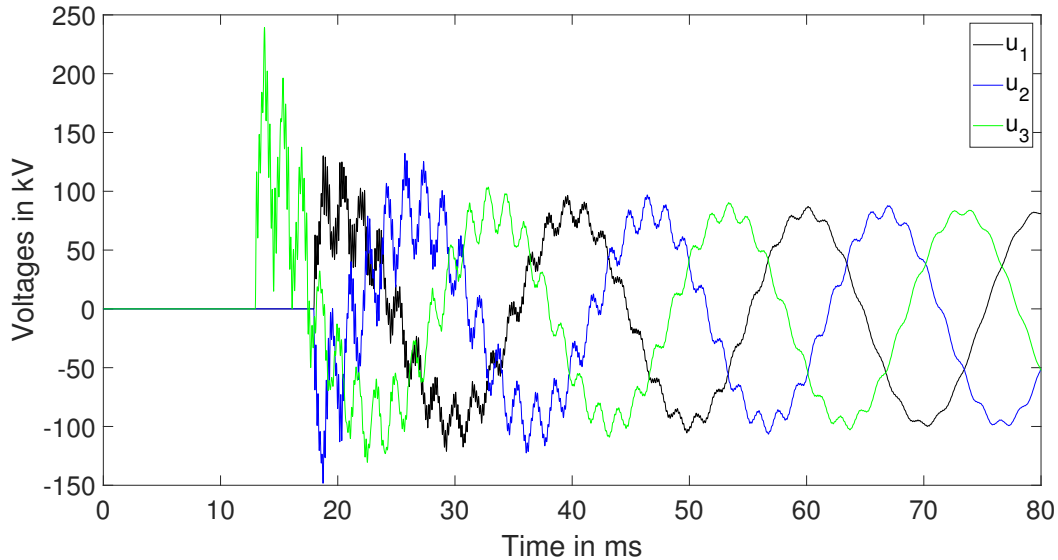


Figure 6.2.: Simulated Switching Voltages before the Circuit Breaker

Figure 6.3 shows an enlargement of the opening process with the transient recovery voltage.

6.2.2. Fourier Transformation of Switching Voltages

In order to detect frequencies, an FFT was made over the first half wave of the operating frequency voltage. This is shown in Figure 6.4 for all three phases.

There are three peaks in particular, the operating frequency and the two significant transient voltages. However, there are also other frequencies, the slower ones being dependent on the overhead line model and the faster ones being more dependent on the cable model.

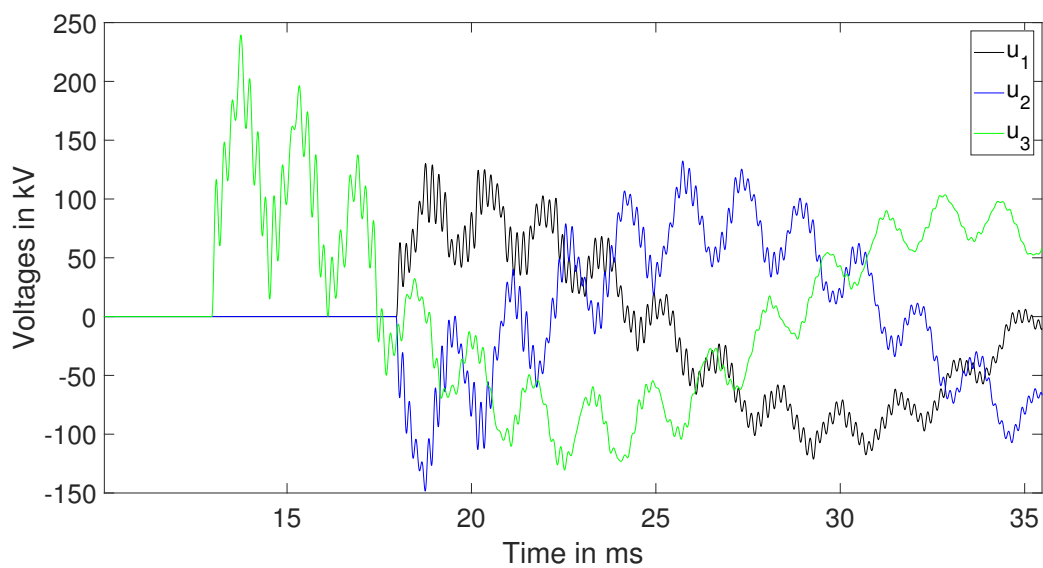


Figure 6.3.: Enlargement of the Opening Process - Simulation

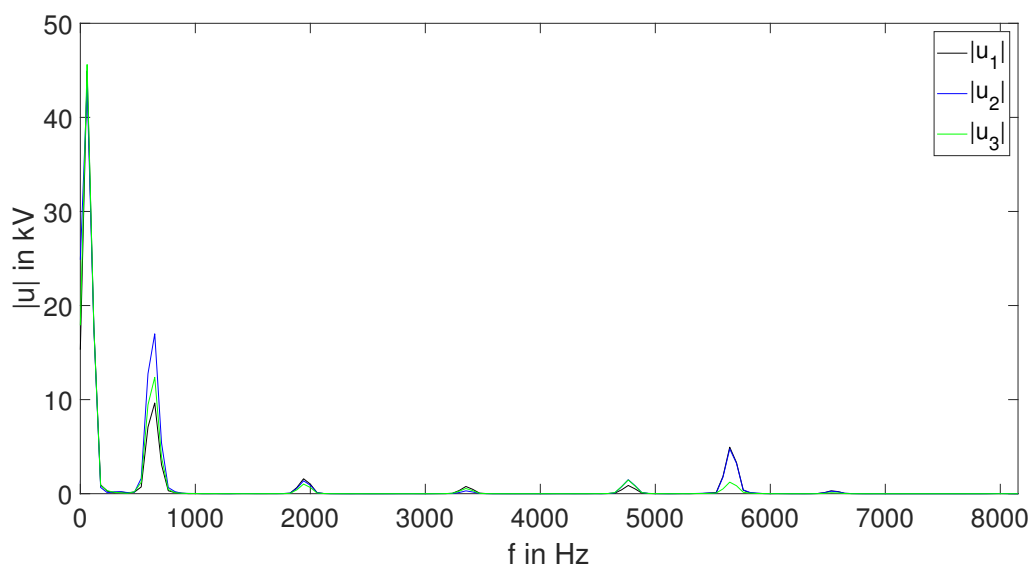


Figure 6.4.: FFT of the Simulated Switching Voltages

6.3. Sensitivity Analysis

6.3.1. Bus Bar Model

For the components from the cable to the circuit breaker under test, as explained in chapter 5.4, a line model with the dimensions of the busbar was used. This was assumed to be 40 meters long and the other components installed were neglected. Initially it was assumed that this section could have a significant influence on the entire construction due to the changed characteristic impedance.

For a better comparison, the parameters were examined as discrete components. Due to the high conductor cross section and the short length, the resistance is very low. This leads to a low attenuation in this section and is independent of the use of frequency dependent or frequency independent models. The inductance and capacitance of the bus bar are also very low compared to the other components. Thus it was found that due to the short length the parameters of this section have hardly any influence on the simulation results.

6.3.2. Transformer Model

The transformer is modelled as explained in chapter 5.5. In addition, capacities C_6 , C_7 and C_8 according to the standard IEEE399-1997 [12] are added for the bushings. In normal operation the 110 kV network is resonantly grounded. In the substation the Peterson coil (indicated with a grey symbol L_1) was available. However, this coil was not used for the real short circuit tests and the neutral point was therefore left open in the simulation as well. Figure 6.5 shows the used transformer model with the additional elements.

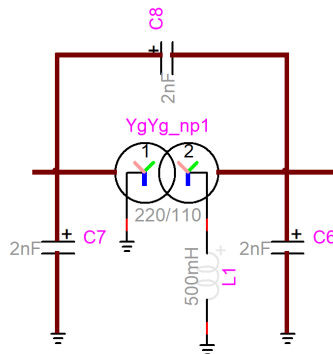


Figure 6.5.: Transformer Model with Capacitances

The transformer is a main element of the setup and has a particular influence on the switching voltages. This is mainly due to the high inductance. In the event of a short circuit, the current is limited mainly by this and the impedance of the overhead line.

Furthermore, the magnetic energy stored in this inductance must be dissipated after the fault has been cleared. This leads to fast transient overvoltages due resonance frequencies with the capacitances on the secondary side of the transformer.

The added capacitances increase the total capacitance which influences the resonance frequencies of the cable and the transformer inductance. Since the frequency is indirectly proportional to the capacitance, the frequency becomes smaller with the capacitances used.

Peterson Coil

The Peterson coil was not used in the measurements, but its impact of the switching voltages in the simulation were investigated. In figure 6.6 the switching voltages with a Peterson Coil of 500 mH can be seen. It is noticeable that the amplitude of the first pole-to-clear voltage stays almost the same, but the other amplitudes are much higher. Also the frequencies of the transients change. This is the case because the Peterson coil influences the zero sequence impedance of the entire system.

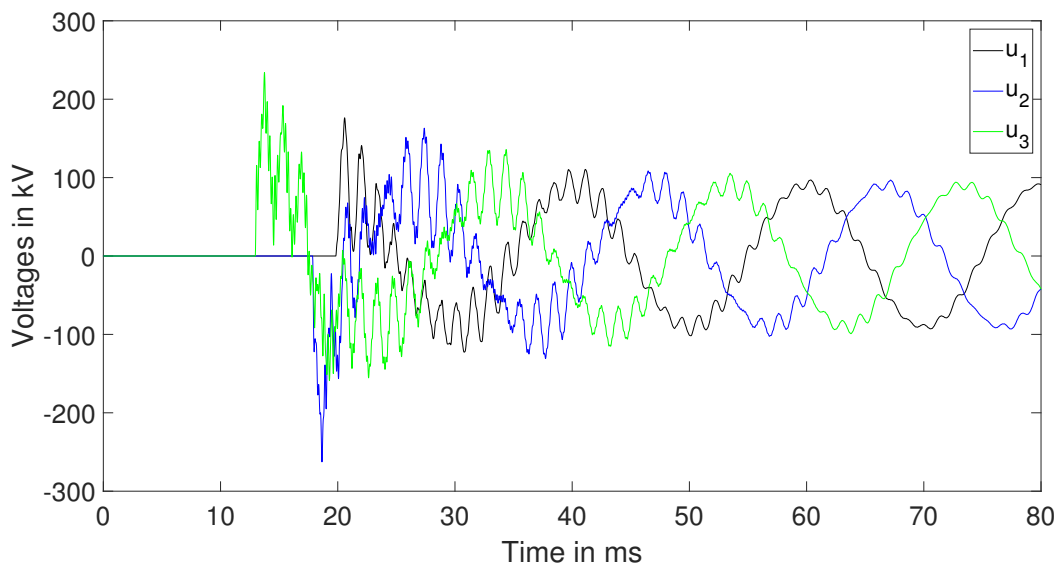


Figure 6.6.: Simulated Voltages with Peterson Coil 500 mH

6.3.3. Cable Model

The cable is another important component for the transient voltages that occur. As already explained in detail in chapter 5.2, different cable models were used for this thesis. These were swapped throughout the entire setup and the changes in the overall result were investigated.

As expected, the damping of the fast frequencies is better with the frequency dependent models due to the increase in resistance. With the models of constant parameters it is slightly weaker. However, the occurring transients differ only in the amplitude level, whereas the frequency remains similar with all models.

Due to the high capacitance of the cable, this is a major factor for the resonance frequencies with the transformer inductance. These two components are the main reason for the fast transient voltage.

As already mentioned there are different ways to connect the cable shields. For the measurements it was chosen to connect the shield wires at each end together and connect the feeder side also to ground. In the EMTP model different configurations were simulated, but for the overall results the shield treatment had hardly any influence.

6.3.4. Line Model

For the overhead line the models as described in chapter 5.3 were used. Each model was used for the simulation and the differences in the results were investigated.

It was found that the slower transient recovery voltage is mainly dependent on the components at the primary side of the transformer. Especially the overhead line is essential because of its length and the resulting high parameters. The constant parameter model also led to a weaker attenuation. Furthermore, it should be mentioned that an extension of the line had no influence on the frequency, since this depends on the characteristic impedance and the propagation speed. However, the signal was attenuated more due to the higher resistance.

6.3.5. Grid Impedance

The grid impedance up to the overhead line is calculated with the short circuit power. An average switching state was chosen and on this basis a power of 5500 MVA was simulated with a load flow calculation program. The X_1/R_1 ratio was assumed to be 10 and the inductance and resistance of the grid were calculated using the following formulas.

$$Z_{grid} = \frac{U_{nominal}^2}{S_{short}} = \frac{(220 \text{ kV})^2}{5500 \text{ MVA}} = 8.8 \Omega \quad (6.1)$$

$$R_{grid} = \sqrt{\frac{Z_{grid}^2}{101}} = \sqrt{\frac{(8.8 \Omega)^2}{101}} = 875.6 \text{ m}\Omega \quad (6.2)$$

$$X_{grid} = 10 \cdot R_{grid} = 10 \cdot 875.6 \text{ m}\Omega = 8.76 \Omega \quad (6.3)$$

$$L_{grid} = \frac{X_{grid}}{2\pi f} = \frac{8.76 \Omega}{2\pi \cdot 50 \text{ Hz}} = 27.87 \text{ mH} \quad (6.4)$$

It is clearly evident that the short circuit power that is used has a high influence factor on the grid impedance. It means that at higher short circuit power the grid impedance is lower. This influence then the assumed inductance and resistance.

The figure 6.7 shows the FFT of the simulated switching voltages of phase one u_1 with variation of the short circuit power. It can be seen that with lower short circuit power especially the slower transients get slower compared to the simulation with 5500 kVA. With higher short circuit power the grid impedance gets lower and this results to higher frequencies. However, it can also be noticed that this variation has hardly any influence at the highest transient. This is the case because the short circuit power changes the parameters on the primary side of the transformer. It can be concluded that the significant slow transient voltage depends on the grid impedance and the overhead line.

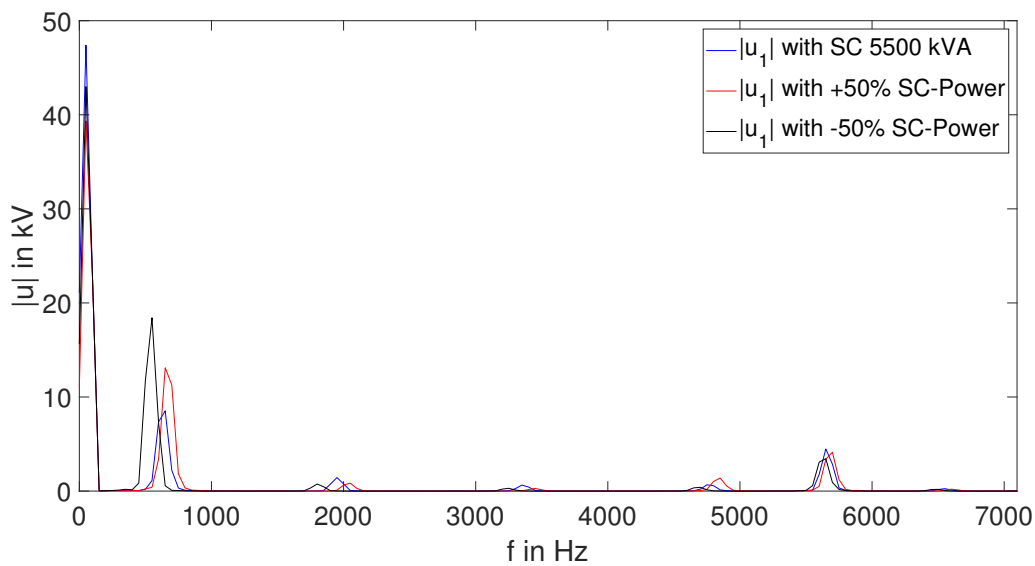


Figure 6.7.: FFT of Simulated Voltages at Different Short Circuit Power

6.3.6. Voltage Dividers

The voltage dividers were modelled very detailed with all components, but also very simplified with the significant capacitance. Therefore only the capacitor C_p which is a factor thousand smaller was used. This neglect of the other elements had hardly any influence on the results. However, the voltage divider itself had an influence on the circuit due to its capacity. It is clearly lower than that of the cable, but it is no longer negligible compared to other components.

In figure 6.8 it can be seen how the capacitance of the voltage dividers influence the frequencies. It can be noticed that the slow transient voltages hardly change, but at the high transient there is a frequency shift. This is the case because with the voltage dividers the capacitance at the secondary side of the transformer increase. Due to the equation for the resonant frequency then the frequency is getting lower.

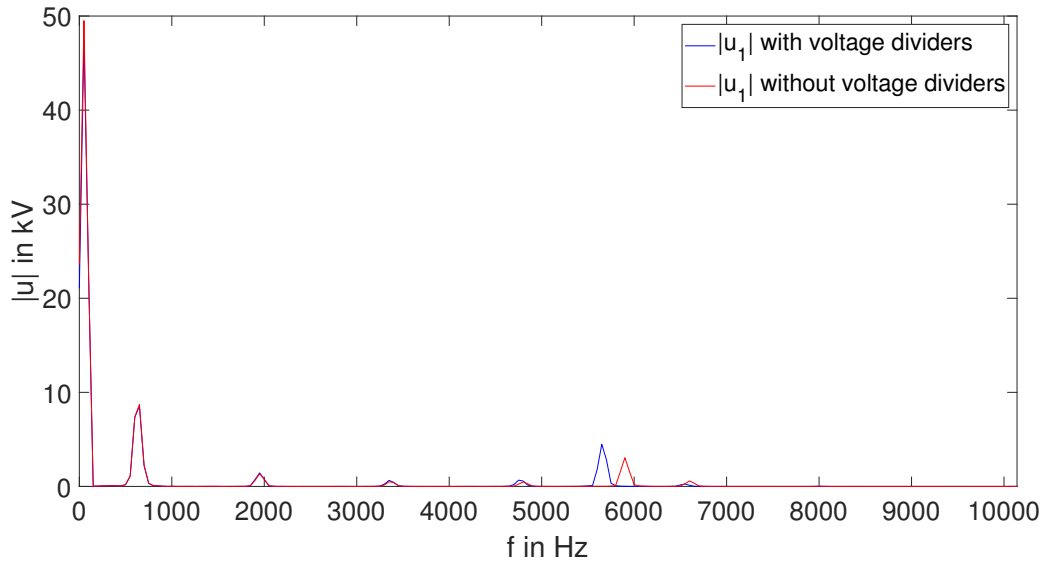


Figure 6.8.: FFT of Simulated Voltages with no Voltage Dividers

6.4. Comparison of Measurement with Simulation

Now that we have described the measurement results from the experiments and the simulated results in more detail, they can be compared qualitatively. In the simulation the transient recovery voltage with two significant non-operating frequencies could be simulated. However, the frequencies of these transient voltages do not correspond exactly to those of the measurement. The amplitudes of the voltages also differ from each other. As sources of inaccuracy the grid impedance and the neglected components were identified.

6.4.1. Influence Grid Impedance

A mean short circuit power was assumed to calculate the grid impedance. This was taken from a simulation of an average switching state. As already mentioned, this impedance has an influence on the slow frequency of the transient recovery voltage at the circuit breaker. However, in order to match the measurement more exactly, the grid impedance has to be known in a more detail way. That means the closer substations with their connections would have to be known and modelled. This was not done due to the high effort and the low added benefit.

6.4.2. Neglect of Components in Substation

Another aspect for the differences between measurement and simulation corresponds to the simplification and neglect of other components existing in the substation. For the distance between the feeders only the bus bar was modelled, but there are also other different measuring devices and switches. Furthermore, the switchgear of the 220 kV

system with the additional components was neglected. All these components have a capacity to ground and a leakage resistance. This has an influence on the frequencies and also on the attenuation of the voltages.

6.4.3. Influence Circuit Breaker for TRV

As already mentioned in EMTP there is a circuit breaker model to add reignitions and restrikes. With this option it could be possible to reproduce the peaks before the breaker clear the fault completely. Unfortunately, it was not possible as part of this thesis to add this effects in the same way as in the measurement. In a future work there can be spend more time on modelling the circuit breaker to add this phenomena.

7. Conclusion

In summary, the aim of this thesis was to analyze the switching overvoltages of a circuit breaker after clarifying a short circuit. Here the measurement setup was set up directly at a substation, which led to very practical results. The measurement results were evaluated and the occurring effects were described in detail.

The transient recovery voltage was of particular focus, whereby two distinct transient frequencies can be clearly seen. The main factors of these occurring voltages were identified by performing a sensitivity analysis. Here, the slow transient is due to the grid impedance and the overhead line leading to the substation. The faster transient mainly depends on the transformer inductance and the capacitances on the secondary side.

Furthermore, the different transmission line models for overhead lines and cables have been investigated. These were models with simple constant parameters up to more sophisticated ones with frequency dependence. It turned out that especially at higher frequencies this difference becomes higher and can no longer be neglected. Moreover, the different input possibilities of the models were discussed.

The results of the entire simulation correspond qualitatively to the measured voltages. The transient recovery voltage at the breaker with the two significant frequencies was reproduced. However, due to assumptions and simplifications, these two frequencies do not correspond exactly to the measurements. This could be improved by closer modelling and addition of a larger part of the whole network. Furthermore, the voltage peaks before the short circuit was cleared completely, can be reproduced with the circuit breaker model for TRV.

As this thesis describes the most important models in more detail and also describes their influence, these knowledge can be applied to future projects with the simulation program EMTP. Furthermore, the most important factors of switching overvoltages were identified and consequently possible countermeasures could be taken.

Bibliography

- [1] *Schaltüberspannung in Schaltanlagen*. Hochschule Zittau-Görlitz, Uwe Schmidt . URL: <http://www.econs-dresden.de/wordpress/wp-content/uploads/symiso-schaltu%CC%88berspannungen-2017.pdf> (cit. on p. 7).
- [2] Andreas Küchler. *Hochspannungstechnik*. Forth Edition. Springer Vieweg, 2017 (cit. on p. 8).
- [3] Hammad Khan et al. “A Novel Island Detection Methodology for the Realization of Smart Grid”. In: *Smart Grid and Renewable Energy* 02 (Jan. 2011). DOI: [10.4236/sgre.2011.24038](https://doi.org/10.4236/sgre.2011.24038) (cit. on pp. 9, 12).
- [4] “IEEE Guide for the Application of Transient Recovery Voltage for AC High-Voltage Circuit Breakers with Rated Maximum Voltage above 1000 V”. In: *IEEE Std C37.011-2019 (Revision of IEEE Std C37.011-2011)* (2019), pp. 1–127 (cit. on p. 10).
- [5] René Smeets; David F. Peelo; Mirsad Kapetanovic; Anton Janssen; Lou van der Sluis. *Switching in Electrical Transmission and Distribution Systems*. First Edition. Wiley, 2014 (cit. on pp. 10, 12).
- [6] Robert Schürhuber. “Switching in Power Systems”. In: *Course Document, Technical University Graz* (2019) (cit. on p. 11).
- [7] Holger Heuermann. *Hochfrequenztechnik*. Third Edition. Springer Vieweg, 2018 (cit. on p. 14).
- [8] EMTPWorks. *Constant Parameter Transmission line*. Dec. 2019 (cit. on pp. 15, 35).
- [9] *Skineffekt*. Elektronik-Kompodium.de . URL: <https://www.elektronik-kompodium.de/sites/grd/1102141.htm> (cit. on pp. 17, 18).
- [10] *Proximity Effect*. ELECTRICAL TECHNOLOGY4U . URL: <http://www.electricaltech4u.com/what-is-proximity-effect/> (cit. on p. 19).
- [11] Bernd R. Oswald Dietrich Oeding. *Elektrische Kraftwerke und Netze*. Eighth Edition. Springer Vieweg, 2016 (cit. on pp. 34, 36, 49).
- [12] “IEEE Recommended Practice for Industrial and Commercial Power Systems Analysis (Brown Book)”. In: *IEEE Std 399-1997* (1998), pp. 1–488 (cit. on p. 58).

A. Appendix

Table A.1.: Electrical Parameters Overhead Line

Parameter	Symbol	Unity	Value
Resistance positive sequence	R_1	Ω/km	0.084
Reactance positive sequence	X_1	Ω/km	0.415
Impedance positive sequence	Z_1	Ω/km	0.423
Resistance zero sequence	R_0	Ω/km	0.233
Reactance zero sequence	X_0	Ω/km	1.066
Impedance zero sequence	Z_0	Ω/km	1.091
Capacitance to earth	C_E	nF/km	5.549
Operating capacitance	C_B	nF/km	8.946
Surge impedance	Z_w	Ω	384

Table A.2.: Conductor Parameters Overhead Line

-	Line conductors	Earth wire
Nominal cross section	340/110 mm^2	120/42 mm^2
Material	Al/Steel	Al/Steel
Diameter	27.9 mm	16.5 mm
Line length	95 km	

Table A.3.: Technical Details Cable

Cross section	Conductor diameter	Insulation thickness	Diameter over insulation	Approx. screen area	Nominal thickness of APL/HDPE sheath	Overall diameter appr.
<i>mm²</i>	mm	mm	mm	<i>mm²</i>	mm	mm
300	20.3	18	60.7	116.3	0.25/3.2	75.6

Table A.4.: Electrical Parameters Cable

Conductor DC resistance at 20°C	Conductor AC resistance at 50 Hz and 90°C	Inductive reactance at 50 Hz and 90°C	Conductor to screen capacitance
Ω/km	Ω/km	Ω/km	$\mu\text{F}/\text{km}$
0.0601	0.078	0.154	0.129
Screen DC resistance at 20°C sheath	Zero sequence resistance at 20°C	Zero sequence reactance at 50 Hz	
Ω/km	Ω/km	Ω/km	
0.162	0.161	0.093	